Cooling tower plume abatement using a coaxial plume structure

Shuo Li[1,*], Ali Moradi[1,2], Brad Vickers[2] and M. R. Flynn[1]

[1] *Department of Mechanical Engineering, University of Alberta, Edmonton, AB T6G 1H9, Canada*

[2] *International Cooling Tower Inc., Edmonton, AB T6N 1C7, Canada*

Abstract

The traditional approach of cooling tower plume abatement is supposed to result in an unsaturated, well-mixed plume with a "top-hat" structure in the radial structure, but this is an idealization that is rarely achieved in practice. Meanwhile, previous analyses have shown that there may be an advantage in specifically separating the wet and dry air streams whereby the corresponding plume is of the coaxial variety with dry air enveloping (and thereby shielding) an inner core of wet air. Given that a detailed understanding of the evolution of coaxial plumes is presently lacking, we derive an analytical model of coaxial plumes in the atmosphere, which includes the effects of possible condensation. Of particular concern is to properly parameterize the entrainment (by turbulent engulfment) of fluid from the inner to the outer plume and vice-versa. We also present and discuss the two different body force formulations that apply in describing the dynamics of the inner plume. Based on the resulting model predictions, we introduce a so-called *resistance factor*, which is defined as the ratio of the average non-dimensional velocity to the average relative humidity. In the context of visible plume abatement, the resistance factor so defined specifies the likelihood of fog formation and/or a recirculation of moist air into the plenum chamber. On the basis of this analysis, we can identify the region of the operating-environmental condition parameter space where a coaxial plume might offer advantages over its uniform counterpart.

Keywords: moist plume; coaxial plume; hybrid cooling tower; plume abatement

1 Introduction

A visible plume is a column of microscopic droplets of condensed water. Hot, moist air emitted from a wet cooling tower cools by entraining cold ambient air and a visible plume, or fog, forms if the plume temperature falls below the dew-point temperature. Though containing no pollutants except in entrained water droplets, which are, in any event, few in number, a visible plume is oftentimes regarded as a nuisance, which is better avoided. This need has led to various strategies for plume abatement (see below) whereas the need to model the fluid- and thermodynamical behavior of cooling tower plumes has produced a voluminous literature on the topic. Indeed, the analytical description of atmospheric plumes, cooling tower and otherwise, dates back to Morton (1957), who formulated a one-dimensional, "top-hat" model of vertically ascending thermal plumes in a moist ambient based on the integral approach of Morton et al (1956) (hereafter referred to as MTT). In the work of Morton (1957) (but not MTT), the potential temperature and density, which are conserved during adiabatic processes, are used in the governing equations. Morton's model, which can predict the height at which fog will begin to form within the ascending plume, was improved upon by Csanady (1971), who included an ambient wind and was the first to note that condensation might

[*]Corresponding author: Shuo Li, `shuo10@ualberta.ca`

occur only over some intermediate range of heights. The subsequent numerical results of Wigley and Slawson (1971) support this conclusion but indicate that whatever condensation does occur must do so relatively close to the stack/plume source. Wigley and Slawson further showed (Wigley and Slawson, 1972 – see also Hanna, 1972; Weil, 1974; and Wigley 1975) that plumes that include condensation rise to greater heights than do plumes in which no fog is formed. Wu and Koh (1978) proposed a merging criteria for the multiple plumes that emanate from adjacent cooling tower cells. Their predictions are in good agreement with corresponding laboratory data on dry plumes (without moisture). Carhart and Policastro (1991) developed the Argonne National Laboratory and University of Illinois (ANL/UI) model (a so-called second-generation model) to resolve select deficiencies of previous integral models e.g. their inability to correctly and simultaneously predict plume bending and dilution. Furthermore, Janicke and Janicke (2001) proposed an integral plume rise model which can be applied to arbitrary wind fields and source conditions.

Based on the above quick review, we now focus on the (hybrid) cooling tower configurations associated with different plume abatement strategies. Arguably the most popular configuration is the so-called parallel path wet/dry or PPWD configuration, which has been deployed commercially for more than 40 years. Lindahl and Jameson (1993) present a detailed description of PPWD towers, for both counter- and crossflow operation. In the former case, wet air exiting the fill section is co-mingled with comparatively dry air exiting heat exchanger bundle(s) (see figure 2.1 below). The two air streams mix in a plenum chamber and are then discharged to the atmosphere by a fan. Although perfect mixing is never achieved in practice, such an idealization serves as a convenient starting point for the development of plume dispersion models. In the crossflow configuration, the strategy is quite different. Here, air flows horizontally through the fill (see figure 2.5 below). Once in the plenum, this wet air stream has a velocity approximately twice that of the dry air and so the opportunity for mixing is (deliberately) limited. As a result, the plumes generated by PPWD crossflow cooling towers tend to be of the co-axial variety with dry air enveloping (and thereby shielding) an inner core of wet air. As illustrated in Figure 10 of Lindahl and Jameson (1993), the coaxial wet/dry plume above a PPWD crossflow tower results in a cone shaped visible plume that disappears at a vertical distance of about two to three fan stack diameters. Alas, a more detailed understanding of the evolution of coaxial plumes is presently lacking. Given this deficit of knowledge, our present goals are twofold: (i) to adapt ideas from Morton (1957), Wu and Koh (1978) and many others and thereby derive an analytical model for coaxial plumes in the atmosphere, and, (ii) to identify that region of the operating condition-environmental condition parameter space for PPWD where a coaxial plume might offer an advantage over its uniform counterpart. Of course, one might prefer a crossflow PPWD tower for other reasons: the lack of static mixing devices within the plenum chamber signifies a smaller pressure drop to be overcome by the fan. Such design- and operation-specific details are not of principal concern here. Rather, our primary focus is on the buoyant convection that occurs above the cooling tower.

The manuscript is arranged as follows. In section 2 we recapitulate the theoretical model germane to uniform plumes encountered in PPWD counterflow towers. Following a discussion of coaxial plume structures in the open literature in section 2.3, we formulate in section 3 the theory for coaxial plumes above PPWD crossflow towers. Thereafter, in section 4, we study the range of process/ambient conditions where a coaxial plume structure offers some advantage with respect to plume abatement. Finally section 5 provides conclusions for the work as a whole and also identifies ideas for future research.

2 Theory for uniform plumes and its application to counterflow cooling towers

Figure 2.1 is a simplified sketch of a PPWD counterflow cooling tower. A dry section that consists of finned tube heat exchangers is added above the wet section, which consists of a spray zone, fill zone and rain zone. Thus warm, less humid air from the dry section and hot, saturated air from the wet section flow into the plenum chamber located just upstream of the axial fan. The two air streams are mixed thoroughly then discharged to the atmosphere with an average relative humidity below saturation. Streng (1998) suggests that the PPWD counterflow cooling tower, with its series connection of the dry and wet sections on the water side and parallel connection of these sections on the air side, produces the most effective overall cooling performance.

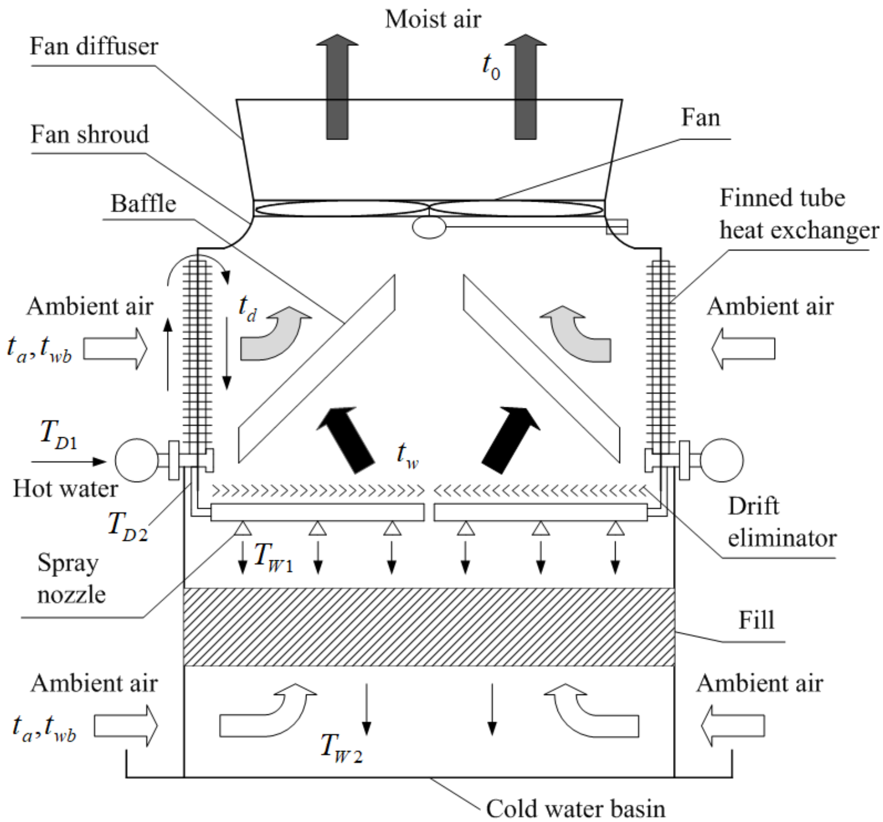

Figure 2.1: Schematic of a PPWD counterflow cooling tower. The white arrows denote the ambient air. The black and light gray arrows denote, respectively, the hot, saturated air from the wet section and the warm, dry air from the dry section. The dark gray arrows at the top of fan shroud denote the resulting well-mixed air stream (We assume complete mixing within the plenum chamber.). In the dry section, t_a is the ambient dry-bulb temperature, t_{wb} is the ambient wet-bulb temperature, t_d is the temperature of the sensibly heated air from the dry section (also called the dry cooling temperature), T_{D1} is the dry section inlet water temperature, T_{D2} is the dry section outlet water temperature, $R_D = T_{D1} - T_{D2}$ is the range temperature in the dry section and $A_D = T_{D2} - t_a$ is the approach temperature in the dry section. For the wet section, t_w is the temperature of the saturated moist air discharged from the drift eliminator, T_{W1} is the wet section inlet water temperature where, ideally, $T_{W1} = T_{D2}$. Moreover, T_{W2} is the wet section outlet water temperature, $R_W = T_{W1} - T_{W2}$ is the range temperature in the wet section and $A_W = T_{W2} - t_{wb}$ is the approach in the dry section. Finally, t_0 is the temperature of the well-mixed air at the top of the fan shroud/base of the (uniform) plume.

To describe the uniform plume that forms above the PPWD counterflow cooling tower illustrated in figure 2.1, we adapt the integral model of Wu and Koh (1978), which allows prediction of the plume temperature, moisture (vapor and liquid phases), vertical velocity, width, and density as well as the visible plume length in case of condensation. The main assumptions are:

(i) Molecular transport is negligible compared to turbulent transport as a result of which (a)

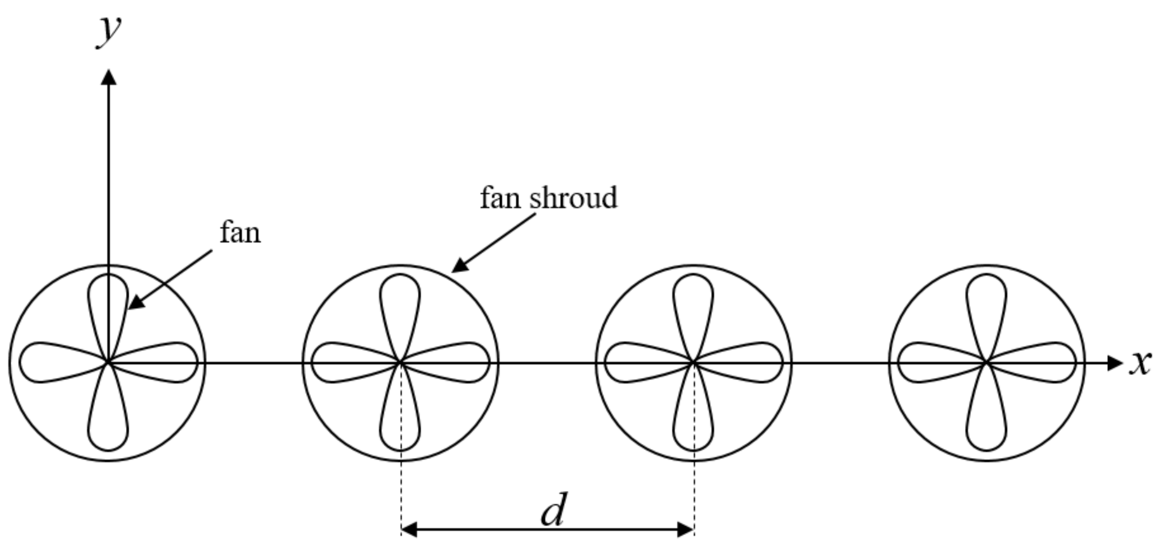

Figure 2.2: The coordinate system associated with a (four cell) cooling tower in a still ambient. The z axis points upwards, i.e. out of the page.

model output is independent of the Reynolds number, and, (b) the Lewis number, defined as the ratio of thermal to mass diffusivity, is unity (Kloppers and Kröger, 2005). Because Le $= 1$, the dilution curve that appears in the psychrometric chart connecting the cooling tower exit to the far field ambient is a straight line.

(ii) The cross-sectional profiles of the plume vertical velocity, temperature, density, vapor and liquid phase moistures are all self-similar. More specifically, plume properties are assumed to exhibit "top-hat" profiles (Davidson, 1986).

(iii) The variation of the plume density is small, i.e. no more than 10%. As such, the Boussinesq approximation can be applied.

(iv) The pressure is hydrostatic throughout the flow field.

(v) The plumes emitted from adjacent cooling tower cells are initially axisymmetric and propagate vertically upwards. At larger elevations, plume merger may occur as a result of which the shape of the combined plume is assumed to be a combination of a finite line plume in the central part and two half axisymmetric plumes at either end. The criterion for plume merger follows from Wu and Koh (1978) and is summarized in Appendix A.

(vi) The ambient is, to a first approximation, assumed to be uniform in temperature and humidity. It is also devoid of liquid phase moisture.

2.1 Formulation

The plan-view schematic of figure 2.2 shows the coordinate system chosen for a typical array of (equidistant) cooling towers. The x-axis is parallel to the line connecting the centers of the cells whereas the z-axis is the vertical axis with $z = 0$ corresponding to the top of the fan shroud.

The conservation equations for mass, momentum, energy and (vapor and liquid phase) moisture are written symbolically as

$$\frac{\mathrm{d}}{\mathrm{d}z}\left\{\int_A \rho_p\, U_p\, \mathrm{d}A\right\} = \rho_a\, E\,, \tag{2.1}$$

$$\frac{\mathrm{d}}{\mathrm{d}z}\left\{\int_A \rho_p\, U_p^2\, \mathrm{d}A\right\} = g\,\int_A \left(\rho_a - \rho_p\right)\, \mathrm{d}A\,, \tag{2.2}$$

$$\frac{\mathrm{d}}{\mathrm{d}z}\left\{\int_A \left(t_p - t_a\right)\, U_p\, \mathrm{d}A\right\} = \int_A \frac{L_v}{c_{pa}}\,\sigma_p\, U_p\, \mathrm{d}A\,, \tag{2.3}$$

$$\frac{\mathrm{d}}{\mathrm{d}z}\left\{\int_A \left[\left(q_p - q_a\right) + \sigma_p\right]\, U_p\, \mathrm{d}A\right\} = 0\,, \tag{2.4}$$

where ρ_p, U_p and A are, respectively, the plume density, vertical velocity, and cross-sectional area. Moreover, q is the specific humidity, t is the air dry-bulb temperature[1], σ is the specific liquid moisture, E specifies the rate of entrainment of external ambient air, g is gravitational acceleration, $L_v(t) = 4.1868\times10^3\,[597.31 - 0.57t]\,\mathrm{J/g}$ is the latent heat of condensation in which t is measured in °C, and $c_{pa} = 1.006\,\mathrm{J/g\,°C}$ is the specific heat capacity of air at constant pressure. The subscripts p and a indicate values in the plume and in the ambient, respectively. According to Taylor's entrainment hypothesis (Morton et al, 1956)

$$E = S\,\gamma\, U_p\,. \tag{2.5}$$

where γ is an entrainment coefficient whose value is approximately 0.117 for axisymmetric plumes and 0.147 for line-source plumes (Bloomfield and Kerr, 2000). Moreover, S is the plume perimeter.

For convenience, we use the virtual temperature when calculating plume densities. The virtual temperature, T_v, corresponds to the temperature of dry air having the same density as a parcel of moist air at an identical pressure (Curry and Webster, 1998; c.f. Monteiro and Torlaschi, 2007). For purposes of including condensation, we adopt the virtual temperature for foggy air[2] and use the following expression, presented by Emanuel (1994):

$$t_v = t\,\left(1 + 0.608q - \sigma\right)\,, \tag{2.6}$$

$$P = \rho_p\, R_a\, t_v\,, \tag{2.7}$$

where t and t_v are measured in Kelvin, P is the total pressure inside/outside the plume and $R_a = 287.058\,\mathrm{J/kg\,K}$ is the gas constant of air. Note that the above definition for t_v incorporates liquid moisture to express the change in bulk density as a result of condensed water.

Applying the Boussinesq approximation and the definition of the virtual temperature, (2.1)–(2.2) can be simplified as,

$$\frac{\mathrm{d}}{\mathrm{d}z}\left\{\int_A U_p\, \mathrm{d}A\right\} = E\,, \tag{2.8}$$

$$\frac{\mathrm{d}}{\mathrm{d}z}\left\{\int_A U_p^2\, \mathrm{d}A\right\} = \int_A g'\, \mathrm{d}A\,, \tag{2.9}$$

where $g' = g\,\left(\frac{t_{v,p}}{t_{v,a}} - 1\right)$ in which $t_{v,p}$ and $t_{v,a}$ are the virtual temperatures of the plume and ambient, respectively.

To simplify the conservation equations, it is helpful to define the plume volume flux Q, momentum flux M, temperature deficiency flux Θ, specific humidity deficiency flux H, and specific liquid

[1] Below the plume origin and consistent with figure 2.1, we use a lowercase t to indicate the temperature of a gas stream and an uppercase T to indicate the temperature of a liquid stream. Above the plume origin, the lowercase t is retained for the temperature of the moist plume and ambient air.

[2] Moist air can be regarded as a limiting case of foggy air where the liquid moisture content is zero, i.e. $\sigma = 0$.

moisture deficiency flux W as follows:

$$Q = \int_A U_p \, \mathrm{d}A \,, \tag{2.10}$$

$$M = \int_A U_p^2 \, \mathrm{d}A \,, \tag{2.11}$$

$$\Theta = \int_A (t_p - t_a) \; U_p \, \mathrm{d}A \,, \tag{2.12}$$

$$H = \int_A (q_p - q_a) \; U_p \, \mathrm{d}A \,, \tag{2.13}$$

$$W = \int_A (\sigma_p - \sigma_a) \; U_p \, \mathrm{d}A \,. \tag{2.14}$$

Recall that, consistent with the top-hat approximation, ρ_p, U_p, t_p, q_p, and σ_p are all constant inside the plume. Note also that assumption (vi) demands that $\sigma_a = 0$. Rewriting the conservation equations using the above variables yields

$$\frac{\mathrm{d}Q}{\mathrm{d}z} = E \,, \tag{2.15}$$

$$\frac{\mathrm{d}M}{\mathrm{d}z} = g \, \frac{Q^2}{M} \left(\frac{t_{v,p}}{t_{v,a}} - 1 \right) \,, \tag{2.16}$$

$$\frac{\mathrm{d}}{\mathrm{d}z} \left(\Theta - \frac{L_v}{c_{pa}} W \right) = 0 \,, \tag{2.17}$$

$$\frac{\mathrm{d}}{\mathrm{d}z} \, (H + W) = 0 \,, \tag{2.18}$$

where $t_{v,p} = \left(t_a + 273.15 + \frac{\Theta}{Q} \right) \left[1 + 0.608 \left(q_a + \frac{H}{Q} \right) - \frac{W}{Q} \right]$ in (2.16).

The system of equations (2.15)–(2.18) constitutes four ordinary differential equations in five unknowns. Model closure is achieved by noting that

$$\begin{aligned} \sigma_p &= 0 \,, && \text{for } q_p < q_{sp} \text{ (dry plume)} \\ q_p &= q_p(t, P) \,, && \text{for } q_p \geq q_{sp} \text{ (wet plume)} \end{aligned} \tag{2.19}$$

where q_{sp} is the saturation specific humidity and P is the total pressure. The former quantity is given by

$$q_{sp}(t, P) = \frac{M_v P_{sv}(t)}{M_a \left[P - P_{sv}(t) \right] + M_v P_{sv}(t)} \,, \tag{2.20}$$

where $M_v = 18.02 \times 10^{-3}$kg/mol is the water molar mass, $M_a = 28.966 \times 10^{-3}$ kg/mol is the air molar mass, and P_{sv} is the saturated vapor pressure. Within the temperature range of 0 to 200°C, P_{sv}, measured in Pa, is given by (ASHRAE, 2013)

$$P_{sv} = e^{C_1/t + C_2 + C_3 t + C_4 t^2 + C_5 t^3 + C_6 \ln t} \,, \tag{2.21}$$

$$\begin{aligned} C_1 &= -5.8002206 \times 10^3 \text{ K} \,, & C_2 &= 1.3914993 \,, \\ C_3 &= -4.8640239 \times 10^{-2} \text{ K}^{-1} \,, & C_4 &= 4.1764768 \times 10^{-5} \text{ K}^{-2} \,, \\ C_5 &= 1.4452093 \times 10^{-8} \text{ K}^{-3} \,, & C_6 &= 6.5459673 \,. \end{aligned}$$

Meanwhile assumption (iv) requires that the total pressure inside the plume changes hydrostatically with elevation, i.e.

$$P = P_0 - \rho_p \, g \, z \,, \tag{2.22}$$

Here, P_0 denotes the pressure at the top of the cooling tower and ρ_p can be calculated using(2.7).

The system of equations (2.15)–(2.18) with the additional constraint (2.19) can be integrated forward in z starting from known (or, in the design stage, estimated) conditions at the cooling tower exit, i.e. $z = 0$. These so-called source conditions can be computed using the following formulas:

$$\begin{aligned} Q_0 &= \frac{\pi}{4}\, D_0^2\, U_0\,, \\ M_0 &= \frac{\pi}{4}\, D_0^2\, U_0^2\,, \\ \Theta_0 - \frac{L_{v,0}}{c_{pa}}\, W_0 &= \frac{\pi}{4}\, D_0^2\, U_0\,(t_0 - t_a)\,, \\ H_0 + W_0 &= \frac{\pi}{4}\, D_0^2\, U_0\ (q_0 - q_a)\ , \end{aligned} \tag{2.23}$$

where a subscript 0 denotes a value measured at the tower exit so that, for instance, D_0 is the initial plume diameter which corresponds to the inner diameter of the fan shroud.

Due to the complexity of the governing equations, no analytical solution can be obtained. The ordinary differential equations (2.15) to (2.18) are instead solved numerically using MATLAB's `ode45` function.

2.2 Representative solutions

We consider a single cooling tower cell and a line array of $n = 9$ cooling tower cells with representative operating and ambient conditions as specified in table 2.1. For reference, the temperatures described in this table are defined in figure 2.1.

Table 2.1: Representative operating and environmental conditions for a single cooling tower cell and a line array of $n = 9$ cells.

Variable name and symbol	**Value (unit)**
Ambient pressure at the top of the cooling tower, P_a	101325 (Pa)
Ambient temperature, t_a	5 (°C)
Ambient relative humidity, RH_a	60 (%)
Wet cooling temperature, t_w	30 (°C)
Dry cooling temperature, t_d	25 (°C)
Stack exit velocity, U_0	6 (m/s)
Stack exit area, A_0	71.3 (m^2)
Distance between cell centers, d	14.3 (m)
Ratio of the dry air mass flux to the wet air mass flux, $\frac{\dot{m}_\mathrm{d}}{\dot{m}_\mathrm{w}}$	0.6 [black curves] 0.3 [red curves]

Analytical results showing the solution of (2.15)–(2.18) are indicated by the curves of figure 2.3. Note the plume excess temperature and height are non-dimensionalized by the source excess temperature $(t_0 - t_a)$ and source plume diameter D_0, respectively. In the case of the black curves, which assume a dry air mass flux to wet air mass flux of $\frac{\dot{m}_\mathrm{d}}{\dot{m}_\mathrm{w}} = 0.6$, panel (b) confirms that there is no condensation during plume dilution; correspondingly the dilution lines on the psychrometric chart never intersect the saturation curve. Rather, the maximum relative humidity of 90.07% occurs at an elevation of $Z = 2.26$ for both single and multiple cell towers. In the multiple cell case, plume merger begins at $Z = 2.90$. The temperature and relative humidity in the merged plume decay more slowly with elevation because merger is associated with a lesser volume of entrained ambient fluid. The vertical velocity (not shown) is therefore greater in the merged plume, a manifestation of the "buoyant enhancement" described by Briggs (1975).

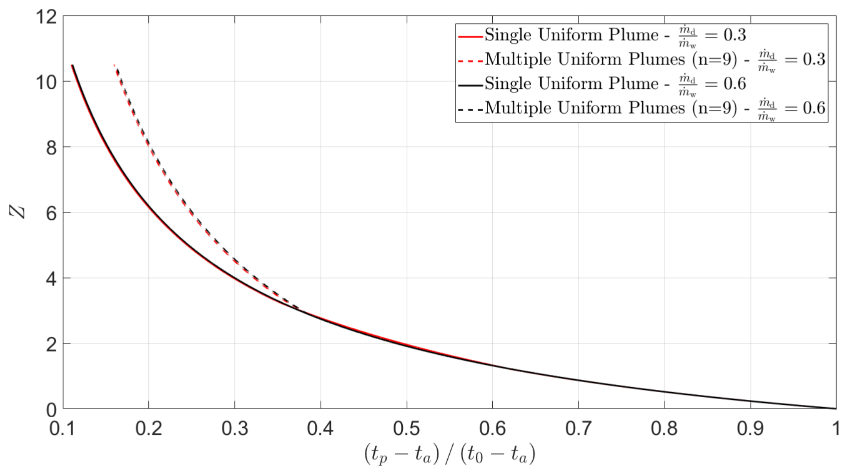

(a)

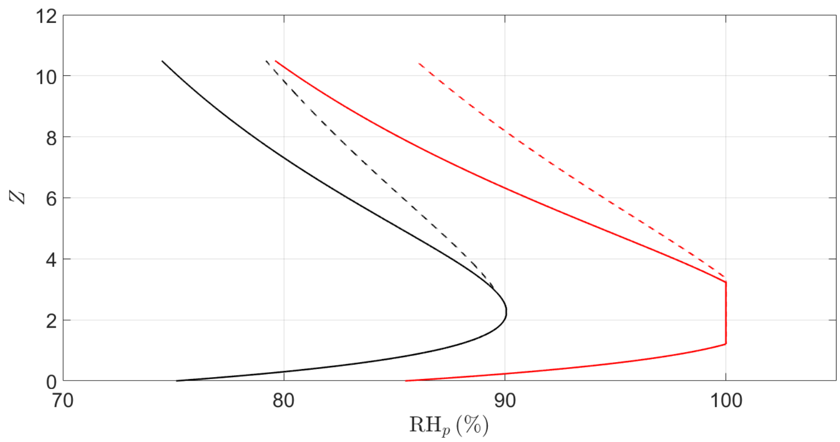

(b)

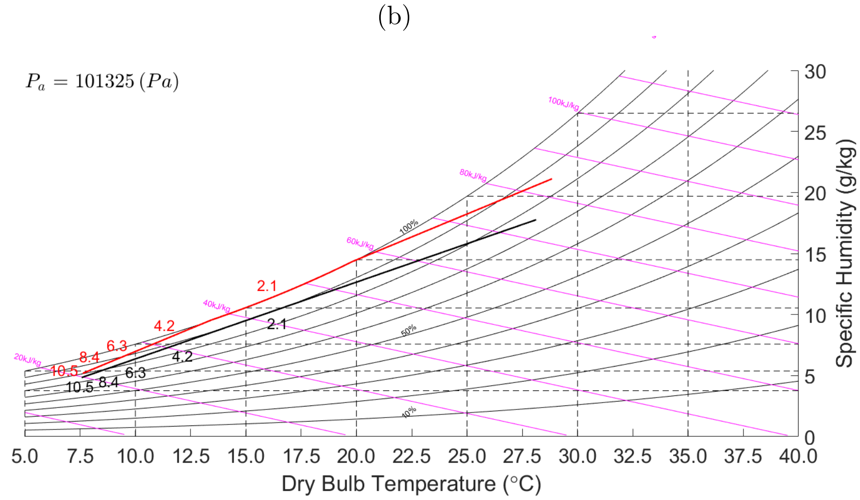

(c)

Figure 2.3: [Color] Non-dimensional plume excess temperature (panel a) and relative humidity (panel b) as functions of height where $Z \equiv z/D_0 = 0$ corresponds to the top of the fan diffuser. Panel (c) shows the plume temperature, specific humidity and the corresponding non-dimensional elevations on the psychrometric chart. Ambient and operating conditions are specified in table 2.1.

Although condensation is absent when $\frac{\dot{m}_\mathrm{d}}{\dot{m}_\mathrm{w}} = 0.6$, figure 2.3 shows that fog will form when this mass flow ratio is reduced to 0.3 corresponding to more limited dry cooling. (Of course, fog may also appear if the ambient temperature or relative humidity are respectively decreased and increased.) As illustrated by the red curves in panel (b) of figure 2.3, the plume undergoes three stages, i.e. invisible, visible and invisible again. In the single cell case, the plume is visible when $1.21 < Z < 3.22$. By contrast, in the $n = 9$ case, the plumes/merged plume is visible when $1.21 < Z < 3.36$. (Plume merger begins at $Z = 2.94$.)

2.3 Discussion

The aforementioned PPWD counterflow towers are supposed to result in a well-mixed plume with a "top-hat" structure in the radial direction, but this is an idealization that is rarely achieved in practice. Generally, mixing is incomplete in the context of hybrid cooling because this mixing, even if aided by static mixing devices, must occur over short vertical distances i.e. the height of the plenum plus fan shroud and fan diffuser. Moreover, the mixing efficacy of the fan from figure 2.1 remains unclear. Whereas the recent numerical study by Takata et al (2016) concludes that the fan could yield complete mixing of the wet and dry airstreams, this finding is contradicted by observation. For instance, Hensley (2009) notes that "the wet and dry air masses tend to follow flow paths through the fan and the combined flow exits the fan cylinder in streamlines". This finding is corroborated by Hubbard et al (2003) who state that "surprisingly little air stream mixing occurs at fan".

Of course, there may be instances in which there is an advantage to specifically separate the wet and dry air streams. Cooling towers based on this idea are often called water conservation cooling towers (Houx et al, 1978; Lindahl and Jameson, 1993; Hensley, 2009). In this configuration, hot water is first sensibly cooled in the dry section, then if additional cooling is needed, the water is then directed to the wet section where evaporative cooling occurs. If no additional cooling is required, the water is instead bypassed directly to the cold water basin thus water conservation is achieved. Houx et al (1978) proposed a water-conserving hybrid cooling tower according to which the ascending plume of wet air is surrounded (or enveloped) by four plumes of ascending dry air. Provided the ambient air temperature is not too low, this configuration is expected to avoid fog formation because the dry air shields the wet air from directly contacting the external ambient. Another benefit associated with this design is that the wet air can rise quickly because its buoyancy is more slowly eroded. Thus the likelihood of recirculating this wet air through the cooling tower is decreased (Kröger, 2004). A similar kind of coaxial wet/dry plume structure can be achieved without the operational headache of running five fans simultaneously by modifying the fan shroud in the manner suggested schematically by figure 2.4 (Koo, 2016a, 2016b). Here, external dry air is drawn into the space between the fan stack and the outer shroud, then mixed with the hot, saturated air discharged by the fan.

Sitting between the cooling tower designs shown in figure 2.1 vs. those of Houx et al (1978), Koo (2016a, 2016b), are, of course, PPWD crossflow towers of the type shown schematically in figure 2.5. According to PPWD crossflow design, the degree of mixing in the plenum chamber is modest and, therefore, the emitted plume is again of coaxial type with (buoyant) wet air occupying the center core.

Motivated by the above summary, we shall, in the sections to follow, develop and apply a theory for coaxial plumes. Although specific reference will be made to PPWD crossflow towers, it should be understood that our governing equations can easily be generalized to cooling towers of the type studied by Houx et al (1978), Koo (2016a, 2016b). Our analysis is motivated by the lack of a robust model for coaxial plumes and will discuss possible advantages of this configuration in the cooling tower/visible plume abatement context. In addition to the reduced probability of recirculation already described, these include, for instance, possibly delaying the onset of condensation.

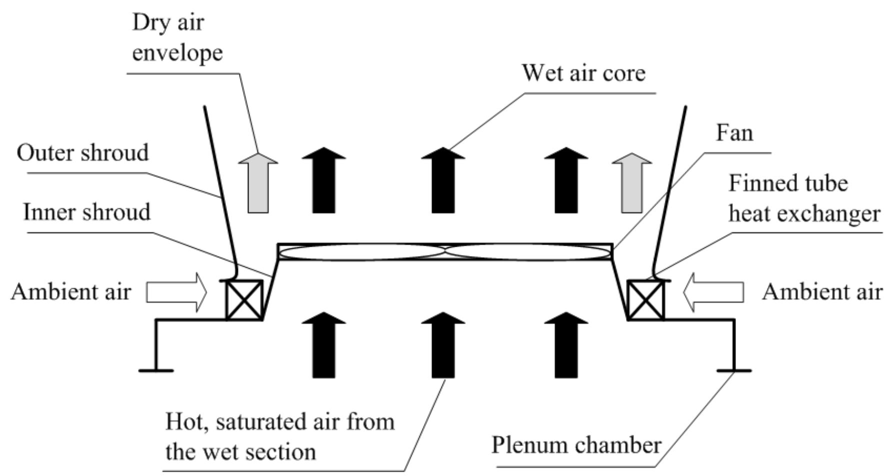

Figure 2.4: The hybrid cooling tower design of Koo (2016a, 2016b). Visible plume abatement is achieved by enveloping the wet air stream within a sheath of drier air.

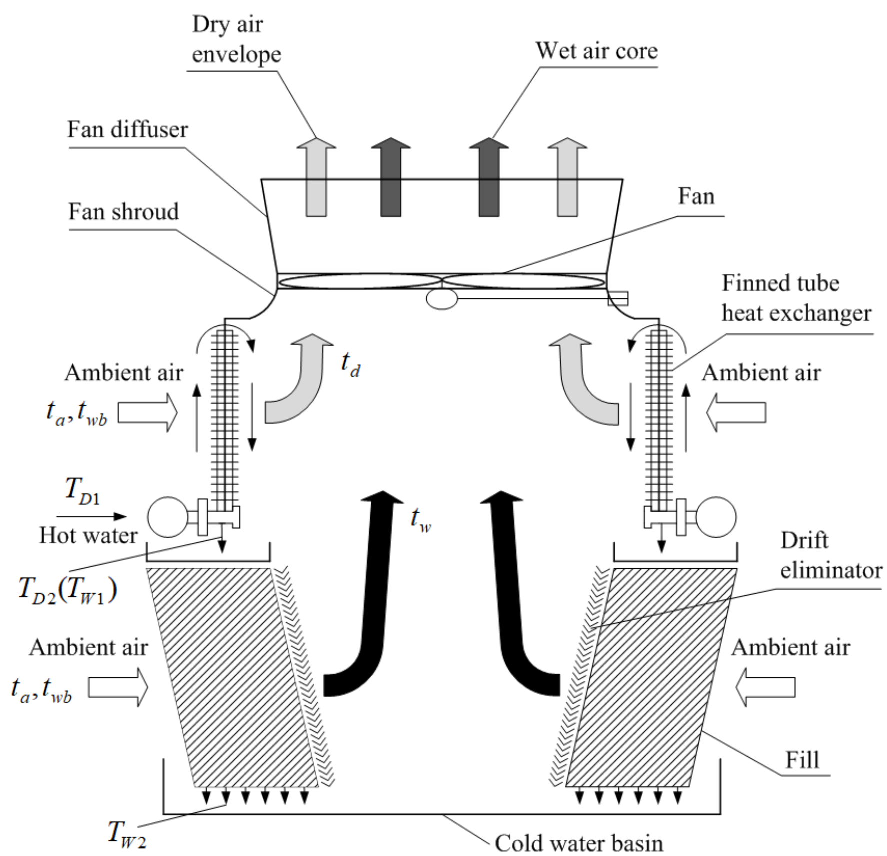

Figure 2.5: As in Figure 2.1 but with a different fill configuration and internal structure inside the plenum chamber. A limited amount of dry air is mixed into the wet air inside the plenum. The remaining fraction is assumed to leave the tower without mixing so that it envelopes the core of wetter air upon discharge to the atmosphere.

3 Theory for coaxial plumes and its application to crossflow cooling towers

3.1 Formulation

The theory of coaxial plumes is developed by analogy with turbulent fountain theory as proposed by McDougall (1981) and subsequently adapted by Bloomfield and Kerr (2000). Before elaborating on this analogy, it is important to note that all previously stated assumptions with the possible exception of assumption (iv) from section 2.1 continue to apply. We further assume that adjacent plumes still merge according to the dynamics described in Appendix A. An important point of difference with the analysis of section 2.1 concerns the body force calculation for the inner plume. Studying a similar coaxial flow problem, McDougall (1981) concluded that there exist two reasonable approaches as outlined below.

The former body force formulation (referred to as BFI by Bloomfield and Kerr, 2000) retains the assumption of a hydrostatic flow. The latter formulation (referred to as BFII by Bloomfield and Kerr, 2000) evaluates the body force of the inner plume relative to the buoyancy of the outer plume, not the ambient. In other words, the body force is determined by computing the density difference between the inner and outer plumes and by considering the acceleration of the outer plume. We defer to an experimental study the determination of which body force formulation is most appropriate in the present context. Suffice it to say for now that the solutions produced using BFI and BFII are very similar in many respects. Moreover, in their careful study of turbulent fountains, Bloomfield and Kerr (2000) determined that formulation BFII provides a moderately better agreement with experimental data than does BFI. As such, we shall apply BFII in the discussion to follow.

A further complication associated with coaxial plumes concerns the entrainment of fluid from the inner to the outer plume and vice-versa. In his investigation of coaxial jets, Morton (1962) argued that the turbulence in the inner jet arose from mean velocity differences between the inner and outer jets, whereas turbulence in the outer jet was due to mean velocity differences between the outer jet and ambient. Adopting the same idea here, and further to figure 3.1, entrainment processes are expressed mathematically as follows:

$$\omega_\alpha = \alpha\,|U_1 - U_2|\,, \quad \omega_\beta = \beta\,U_2\,, \quad \omega_\gamma = \gamma\,U_2\,. \tag{3.1}$$

Here ω_α, ω_β and ω_γ are the entrainment velocities from the outer plume to the inner plume, from the inner plume to the outer plume and from the ambient to the outer plume, respectively. Furthermore, U_1 and U_2 are the respective mean velocities of the inner and outer plumes. Regarding the values of the entrainment coefficients in figure 3.1, we refer to Bloomfield and Kerr (2000) and assume that $\alpha = 0.085$ and $\beta = \gamma = 0.117$. These values are considered to apply up to the point of (outer) plume merger, above which γ is increased to 0.147 corresponding to a pure line plume (List, 1982).

Given (3.1), the conservation of volume, energy and moisture for the inner and outer plumes are respectively expressed as follows:

$$\frac{\mathrm{d}}{\mathrm{d}z}\left\{\int_{A_1} \rho_1\,U_1\,\mathrm{d}A\right\} = \rho_2\,c_1\,\omega_\alpha - \rho_1\,c_1\,\omega_\beta\,, \tag{3.2}$$

$$\frac{\mathrm{d}}{\mathrm{d}z}\left\{\int_{A_2} \rho_2\,U_2\,\mathrm{d}A\right\} = \rho_1\,c_1\,\omega_\beta - \rho_2\,c_1\,\omega_\alpha + \rho_a\,c_2\,\omega_\gamma\,, \tag{3.3}$$

$$\begin{aligned}\frac{\mathrm{d}}{\mathrm{d}z}\left\{\int_{A_1} (t_1 - t_a)\,U_1\,\mathrm{d}A\right\} &= c_1\,\omega_\alpha\,\left(t_2 - t_a - \sigma_2\,\frac{L_{v,2}}{c_{pa}}\right) - c_1\,\omega_\beta\,\left(t_1 - t_a - \sigma_1\,\frac{L_{v,1}}{c_{pa}}\right)\\ &\quad + \frac{\mathrm{d}}{\mathrm{d}z}\left\{\int_{A_1} \frac{L_{v,1}}{c_{pa}}\,\sigma_1\,U_1\,\mathrm{d}A\right\}\,,\end{aligned} \tag{3.4}$$

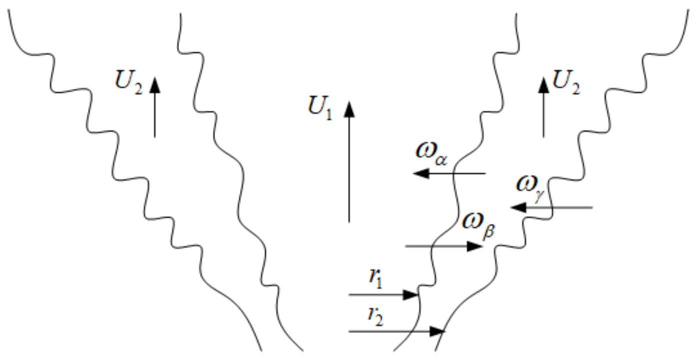

Figure 3.1: Coaxial plume structure. Entrainment from the outer plume to the inner plume, from the inner to the outer plume and from the ambient to the outer plume are parameterized by entrainment coefficients α, β and γ, respectively. Meanwhile, r_1 and r_2 are the respective characteristic radii for the inner and outer plumes.

$$\begin{aligned}\frac{\mathrm{d}}{\mathrm{d}z}\left\{\int_{A_2}(t_2-t_a)\,U_2\,\mathrm{d}A\right\} &= c_1\,\omega_\beta\left(t_1-t_a-\sigma_1\,\frac{L_{v,1}}{c_{pa}}\right)-c_1\,\omega_\alpha\left(t_2-t_a-\sigma_2\,\frac{L_{v,2}}{c_{pa}}\right)\\ &\quad+\frac{\mathrm{d}}{\mathrm{d}z}\left\{\int_{A_2}\frac{L_{v,2}}{c_{pa}}\,\sigma_2\,U_2\,\mathrm{d}A\right\}\,,\end{aligned} \tag{3.5}$$

$$\frac{\mathrm{d}}{\mathrm{d}z}\left\{\int_{A_1}(q_1-q_a+\sigma_1)\,U_1\,\mathrm{d}A\right\}=c_1\,\omega_\alpha\,(q_2-q_a+\sigma_2)-c_1\,\omega_\beta\,(q_1-q_a+\sigma_1)\,, \tag{3.6}$$

$$\frac{\mathrm{d}}{\mathrm{d}z}\left\{\int_{A_2}(q_2-q_a+\sigma_2)\,U_2\,\mathrm{d}A\right\}=c_1\,\omega_\beta\,(q_1-t_a+\sigma_1)-c_1\,\omega_\alpha\,(q_2-q_a+\sigma_2)\,. \tag{3.7}$$

Here, the geometric parameters c_1, c_2, A_1 and A_2 are defined as $c_1=2\pi r_1$ and $c_2=2\pi r_2$, $A_1=\pi r_1^2$ and $A_2=\pi\left(r_2^2-r_1^2\right)$.

Equations (3.2)–(3.7) must be coupled with equations describing momentum conservation. Under the BFII formulation, the momentum conservation equation for the inner plume is

$$\frac{\mathrm{d}}{\mathrm{d}z}\left\{\int_{A_1}\rho_1\,U_1^2\,\mathrm{d}A\right\}=A_1\left[g\,(\rho_2-\rho_1)+\rho_1\,U_2\,\frac{\mathrm{d}U_2}{\mathrm{d}z}\right]+c_1\,\rho_2\,\omega_\alpha\,U_2-c_1\,\rho_1\,\omega_\beta\,U_1\,, \tag{3.8}$$

where $U_2\,\frac{\mathrm{d}U_2}{\mathrm{d}z}$ is the acceleration of the outer plume. To derive the analogue expression for the outer plume, it is helpful to first consider momentum conservation for the coaxial plume as a whole, by which we write

$$\frac{\mathrm{d}}{\mathrm{d}z}\left\{\int_{A_1}\rho_1\,U_1^2\,\mathrm{d}A+\int_{A_2}\rho_2\,U_2^2\,\mathrm{d}A\right\}=g\,A_1\,(\rho_a-\rho_1)+g\,A_2\,(\rho_a-\rho_2)\,. \tag{3.9}$$

Subtracting (3.8) from (3.9) then yields

$$\begin{aligned}\frac{\mathrm{d}}{\mathrm{d}z}\left\{\int_{A_2}\rho_2\,U_2^2\,\mathrm{d}A\right\}&=A_1\left[g\,(\rho_a-\rho_2)-\rho_1\,U_2\,\frac{\mathrm{d}U_2}{\mathrm{d}z}\right]+g\,A_2\,(\rho_a-\rho_2)\\ &\quad+c_1\,\rho_1\,\omega_\beta\,U_1-c_1\,\rho_2\,\omega_\alpha\,U_2\,.\end{aligned} \tag{3.10}$$

Analogous to section 2.1, it is helpful to define an equivalent set of integral parameters as follows:

$$Q_1=\int_{A_1}U_1\,\mathrm{d}A\,,\qquad\qquad Q_2=\int_{A_2}U_2\,\mathrm{d}A\,, \tag{3.11}$$

$$M_1 = \int_{A_1} U_1^2 \,\mathrm{d}A\,, \qquad M_2 = \int_{A_2} U_2^2 \,\mathrm{d}A\,, \tag{3.12}$$

$$\Theta_1 = \int_{A_1} (t_1 - t_a)\, U_1 \,\mathrm{d}A\,, \qquad \Theta_2 = \int_{A_2} (t_2 - t_a)\, U_2 \,\mathrm{d}A\,, \tag{3.13}$$

$$H_1 = \int_{A_1} (q_1 - q_a)\, U_1 \,\mathrm{d}A\,, \qquad H_2 = \int_{A_2} (q_2 - q_a)\, U_2 \,\mathrm{d}A\,, \tag{3.14}$$

$$W_1 = \int_{A_1} \sigma_1\, U_1 \,\mathrm{d}A\,, \qquad W_2 = \int_{A_2} \sigma_2\, U_2 \,\mathrm{d}A\,, \tag{3.15}$$

where, consistent with figure 3.1, subscripts 1 and 2 refer to the inner and outer plumes, respectively.

The aforementioned conservation equations for volume, energy and moisture then become

$$\frac{\mathrm{d}Q_1}{\mathrm{d}z} = c_1\,\left(\omega_\alpha - \omega_\beta\right)\,, \tag{3.16}$$

$$\frac{\mathrm{d}Q_2}{\mathrm{d}z} = c_1\,\left(\omega_\beta - \omega_\alpha\right) + c_2\,\omega_\gamma\,, \tag{3.17}$$

$$\frac{\mathrm{d}}{\mathrm{d}z}\left(\Theta_1 - \frac{L_{v,1}}{c_{pa}}\,W_1\right) = c_1\,\omega_\alpha\,\left(t_2 - t_a - \sigma_2\,\frac{L_{v,2}}{c_{pa}}\right) - c_1\,\omega_\beta\,\left(t_1 - t_a - \sigma_1\,\frac{L_{v,1}}{c_{pa}}\right)\,, \tag{3.18}$$

$$\frac{\mathrm{d}}{\mathrm{d}z}\left(\Theta_2 - \frac{L_{v,2}}{c_{pa}}\,W_2\right) = c_1\,\omega_\beta\,\left(t_1 - t_a - \sigma_1\,\frac{L_{v,1}}{c_{pa}}\right) - c_1\,\omega_\alpha\,\left(t_2 - t_a - \sigma_2\,\frac{L_{v,2}}{c_{pa}}\right)\,, \tag{3.19}$$

$$\frac{\mathrm{d}}{\mathrm{d}z}\left(H_1 + W_1\right) = c_1\,\omega_\alpha\,\left(q_2 - q_a + \sigma_2\right) - c_1\,\omega_\beta\,\left(q_1 - q_a + \sigma_1\right)\,, \tag{3.20}$$

$$\frac{\mathrm{d}}{\mathrm{d}z}\left(H_2 + W_2\right) = c_1\,\omega_\beta\,\left(q_1 - q_a + \sigma_1\right) - c_1\,\omega_\alpha\,\left(q_2 - q_a + \sigma_2\right)\,. \tag{3.21}$$

Similarly, the momentum conservation equations assuming a BFII formulation are rewritten

$$\frac{\mathrm{d}M_1}{\mathrm{d}z} = A_1\,\left(g_1' - g_2' + U_2\,\frac{\mathrm{d}U_2}{\mathrm{d}z}\right) + c_1\,\left(\omega_\alpha\,U_2 - \omega_\beta\,U_1\right)\,, \tag{3.22}$$

$$\frac{\mathrm{d}M_2}{\mathrm{d}z} = A_1\,\left(g_2' - U_2\,\frac{\mathrm{d}U_2}{\mathrm{d}z}\right) + g_2'\,A_2 + c_1\,\left(\omega_\beta\,U_1 - \omega_\alpha\,U_2\right)\,, \tag{3.23}$$

where $g_1' = g\,\left(\frac{P_2}{P_1}\,\frac{t_{v,1}}{t_{v,a}} - 1\right)$ and $g_2' = g\,\left(\frac{t_{v,2}}{t_{v,a}} - 1\right)$, in which $t_{v,1}$ and $t_{v,2}$ are the virtual temperatures of the inner and outer plumes, respectively. Mathematically, the total pressure, P_1, of the inner plume can be computed from

$$\frac{\mathrm{d}P_1}{\mathrm{d}z} = -g\,\rho_2 - \rho_a\,U_2\,\frac{\mathrm{d}U_2}{\mathrm{d}z}. \tag{3.24}$$

Meanwhile, the (hydrostatic) pressure of the outer plume, P_2, can be determined by trivial adaptation of (2.22).

As before, (2.19) must be used to close the governing equations. Finally, the source conditions for the coaxial plume are as follows:

$$\begin{aligned}
Q_{10} &= A_{10}\,U_{10}\,, & Q_{20} &= A_{20}\,U_{20}\,,\\
M_{10} &= A_{10}\,U_{10}^2\,, & M_{20} &= A_{20}\,U_{20}^2\,,\\
\Theta_{10} - \frac{L_{v,10}}{c_{pa}}\,W_{10} &= A_{10}\,U_{10}\,\left(t_{10} - t_a\right)\,, & \Theta_{20} - \frac{L_{v,20}}{c_{pa}}\,W_{20} &= A_{20}\,U_{20}\,(t_{20} - t_a)\,,\\
H_{10} + W_{10} &= A_{10}\,U_{10}\,\left(q_{10} - q_a\right)\,, & H_{20} + W_{20} &= A_{20}\,U_{20}\,\left(q_{20} - q_a\right).
\end{aligned} \tag{3.25}$$

3.2 Representative solutions

Further to the discussion in section 2.3, we consider in this section a PPWD crossflow tower such as that shown schematically in figure 2.5. As described previously, only modest mixing is supposed to occur in the plenum. The degree of mixing shall be varied in the calculations to follow. More precisely, we shall allow either 5%, 50% or 95% of the dry air to be mixed into the wet air stream below the top of the fan shroud[3]. To make a fair comparison with the results of section 2, we consider the same operating and ambient conditions as shown in table 2.1. We further assume that vertical velocities are spatially-uniform at the top of the fan shroud. As a result, and in comparing the source volume flux of the inner vs. the outer plume, one must consider the proportion of the cross section occupied by each air stream. This proportion is, of course, directly related to the aforementioned mixing fraction.

For the case with $\frac{\dot{m}_{\rm d}}{\dot{m}_{\rm w}} = 0.6$, we present in figure 3.2 plume radii, vertical velocities and reduced gravities for both the inner and outer plumes. For ease of interpretation, we limit ourselves in figure 3.2 to two bookend values for the dry air mixing fraction, namely 5% and 95%. These values correspond to a thick and thin outer plume, respectively. Attention is likewise restricted to a single cooling tower cell; the scenario of multiple cells and the concomitant complication of plume merger shall be investigated later.

Figure 3.2 a indicates that the outer plume expands continuously whereas the inner plume shrinks until it vanishes at some point above the source. For instance, for a dry air mixing fraction (DAMF) of 5%, the inner plume is totally engulfed by the outer plume at an elevation of $Z_{c,\,5\%} = 5.67$. Analogous to the coaxial turbulent jets studied by Morton (1962), below this critical (or "cut-off") height, the inner and outer plumes exhibit considerable differences of velocity (figure 3.2 b) and density (figure 3.2 c). The inner and outer plumes are therefore expected to be demonstrably different one from the other. For the opposite limiting case having a DAMF of 95%, the outer plume starts off very thin, but progressively expands as a result of fluid entrainment. The inner plume again diminishes in radius, but does so over a comparatively large vertical distance.

Because α, β and γ are derived from a study of turbulent fountains (Bloomfield and Kerr, 2000), a sensitivity analysis of the results to variations in the values of the entrainment coefficients is warranted. As shown in table 3.1, we use as reference values $\alpha = 0.085$, $\beta = 0.117$ and $\gamma = 0.117$ then investigate the effect of changing each entrainment coefficient one-by-one. The trends of the data from table 3.1 are as expected with by far the greatest sensitivity arising in the case of the numerical value of β. To wit, $Z_{c,\,5\%}$ increases by a factor of 2.6 when β decreases from 0.117 (axisymmetric plume) to 0.076 (axisymmetric jet). By contrast, increasing β from 0.117 to 0.147 (line plume) causes $Z_{c,\,5\%}$ to decrease from 5.67 to 3.84. Increasing β causes more hot, humid air from the inner plume to be mixed into the outer plume. This has the effect of hastening the disappearance of the inner plume while slowing the dilution and deceleration of the outer plume.

Table 3.1: Sensitivity of $Z_{c,\,5\%}$ to variations in the values of the entrainment coefficients α, β and γ.

Entrainment coefficients	$\mathbf{Z_{c,\,5\%}}$
$\alpha = 0.085$, $\beta = 0.117$ & $\gamma = 0.117$	5.67 (reference)
$\alpha = 0.076$, $\beta = 0.117$ & $\gamma = 0.117$	5.56
$\alpha = 0.117$, $\beta = 0.117$ & $\gamma = 0.117$	6.07
$\alpha = 0.085$, $\beta = 0.076$ & $\gamma = 0.117$	14.82
$\alpha = 0.085$, $\beta = 0.147$ & $\gamma = 0.117$	3.84
$\alpha = 0.085$, $\beta = 0.117$ & $\gamma = 0.076$	4.47
$\alpha = 0.085$, $\beta = 0.117$ & $\gamma = 0.147$	6.80

A distinguishing feature of figure 3.2 b is that the inner plume velocity first decreases then in-

[3]Throughout our analysis, we assume that some fraction of the dry air is mixed into the wet air, but not vice versa. This assumption is based on the fact that the wet air stream at the center of the cooling tower is supposed to have a comparatively low pressure. As a consequence, this wet air stream naturally entrains some dry air into its core.

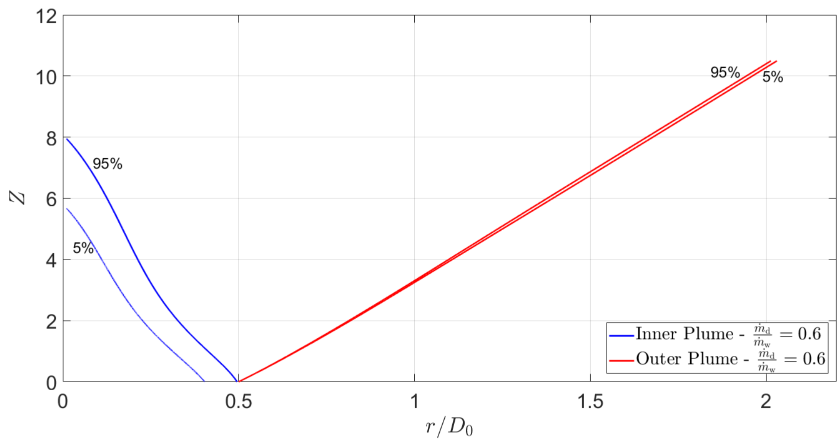

(a)

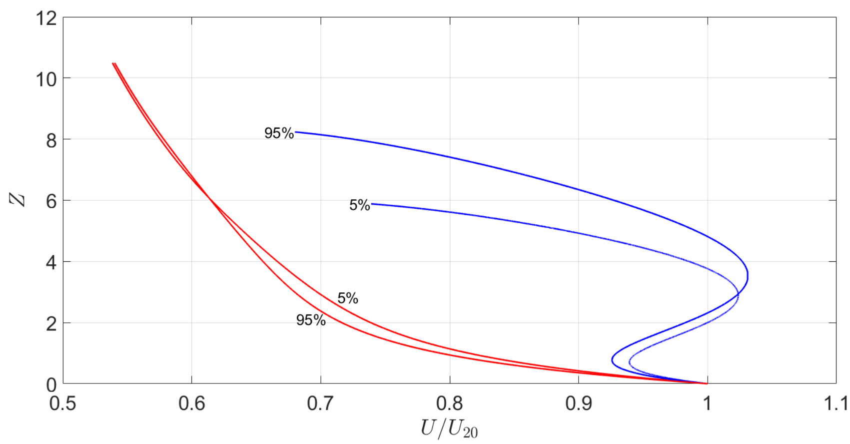

(b)

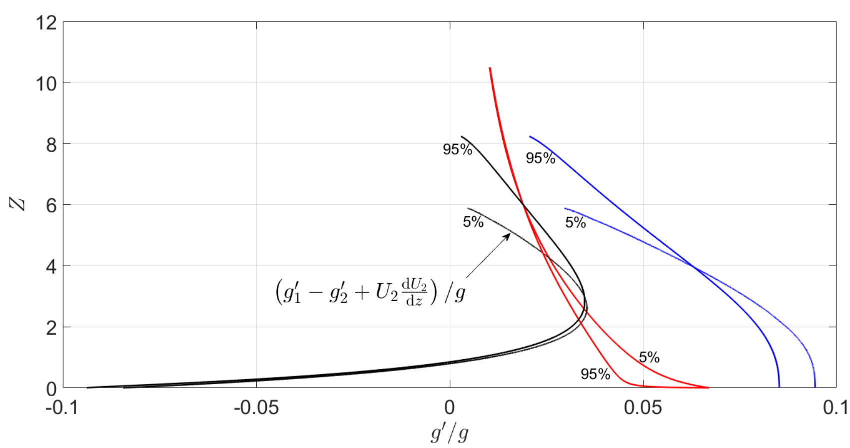

(c)

Figure 3.2: [Color] Non-dimensional plume radii (panel a), vertical velocities (panel b) and reduced gravities (panel c) as functions of height. The solid black curves in panel c denote the non-dimensional body force $\left(g_1' - g_2' + U_2 \frac{\mathrm{d}U_2}{\mathrm{d}z}\right)/g$ in the inner plume. Labels of 5% and 95% denote the dry air mixing fraction (DAMF).

creases then decreases again. This behavior speaks, in part, to the influence of the source conditions and is qualitatively different from that documented by Morton (1962) who studied coaxial jets but did not observe the initial decrease of velocity – see his figure 3. As illustrated by the black dashed curves of figure 3.2 c, $g_1' - g_2' + U_2\frac{\mathrm{d}U_2}{\mathrm{d}z}$, which appears on the right-hand side of (3.22), is initially negative, but increases rapidly owing to the deceleration of the outer plume. When $Z = 0.72$, $g_1' - g_2' + U_2\frac{\mathrm{d}U_2}{\mathrm{d}z}$ changes sign and the inner plume velocity begins gradually to increase. Finally, for $Z \geq 2.96$, the inner plume velocity falls rapidly until such time as the inner plume disappears This is due to the fact that the entrainment of outer plume and, by extension, ambient fluid come to dominate the dynamics of the inner plume. As further evidence of the importance of entrainment, note that differences of velocity and buoyancy between the inner and outer plumes diminish significantly just before the disappearance of the inner plume. As noted above, this disappearance is significantly delayed when the outer plume is initially very thin (5% DAMF). Of course, whatever the initial sizes of the inner and outer plumes, there remains a considerable transport of mass into the latter, which is consistent with the results of coaxial turbulent jets by Morton (1962).

An obvious limitation associated with figure 3.2 is that it does not examine humidity variations for the inner or outer plumes. This deficiency is rectified in figure 3.3, which considers the evolution of the plumes in terms of dynamics and psychrometrics and which now also includes a DAMF of 50%. To be consistent with figure 3.2 and the operating and ambient conditions studied in section 2.2, figure 3.3 again assumes $\frac{\dot{m}_\mathrm{d}}{\dot{m}_\mathrm{w}} = 0.6$. Figure 3.3 a shows that initially the non-dimensional excess temperature $(t_p - t_a)\,/\,(t_{20} - t_a)$ of the outer plume drops sharply because the outer plume becomes diluted by ambient fluid; a much slower initial decrease is noted in the case of the inner plume. Figure 3.3 b indicates that, as expected, the inner plume relative humidity (RH) decreases with increasing DAMF. When the mixing of the dry and wet air streams is severely curtailed i.e. the DAMF is only 5%, condensation is anticipated. Consistent with the blue curves of figure 3.3 a, the relative humidity of the inner plume remains approximately constant below $Z = 1$, then begins to increase as the relative humidity of the outer plume rises sharply. The subsequent decrease in the inner plume relative humidity results from the fact that the outer plume eventually becomes quite dry, i.e. it approaches the psychrometric condition of the ambient air. With respect to the outer plumes there exist below $Z = 2$ considerable deviations in the relative humidities between the 5% and 95% DAMF cases. For instance, at an elevation of $Z = 0.5$, the corresponding relative humidities of the outer plumes are 57.9% (5% DAMF), 67.1% (50% DAMF) and 86.7% (95% DAMF).

Figure 3.3 c presents a very different dilution process on the psychrometric chart compared to the single straight line characteristic of the uniform plume case. Within a short distance above the cooling tower, the outer plume gains humidity because of the entrainment of large volumes of inner plume fluid. Obviously, this process cannot continue indefinitely and the effect of this humidity gain is soon outweighed by the dilution of ambient air. In a similar fashion, the inner plume is gradually consumed rather than diluted by the outer plume. As a result, any fog that is produced in the inner plume will become entrained into the outer plume where evaporation of these water droplets will very quickly occur.

For the case with $\frac{\dot{m}_\mathrm{d}}{\dot{m}_\mathrm{w}} = 0.3$, figure 3.4 illustrates the non-dimensional plume radii, vertical velocities and reduced gravities as functions of height. In contrast to figures 3.2 and 3.3, here we consider only a single value for the DAMF (of 5%), but now specifically investigate differences between the single and multiple cooling tower cell cases. While the single cell results are similar to those in figure 3.2, the results of figure 3.4 c with multiple cells ($n = 9$) show clearly that merged plumes are more buoyant than individual (axisymmetric) plumes. As such, there is an increase in the outer plume rise velocity when $Z = 2.99$ (figure 3.4 b). For still larger Z, the outer plume rise velocity begins to decrease again at about the point where after the inner plume disappears.

Figure 3.5 a shows the same decreasing profiles as those in figure 3.3 a now with a smaller dry to wet air mass flux ratio: the differences among the 5%, 50% and 95% DAMF cases are now less

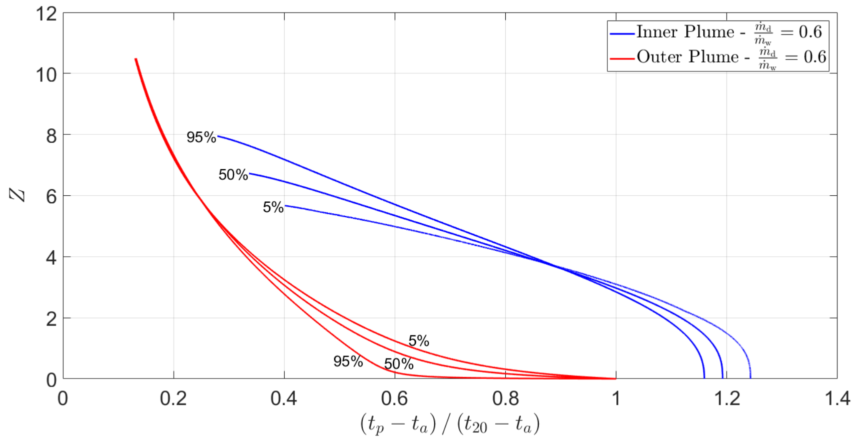

(a)

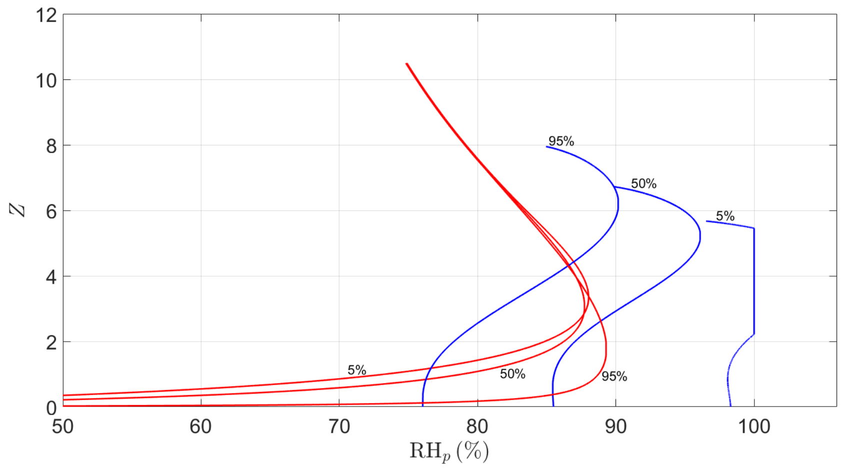

(b)

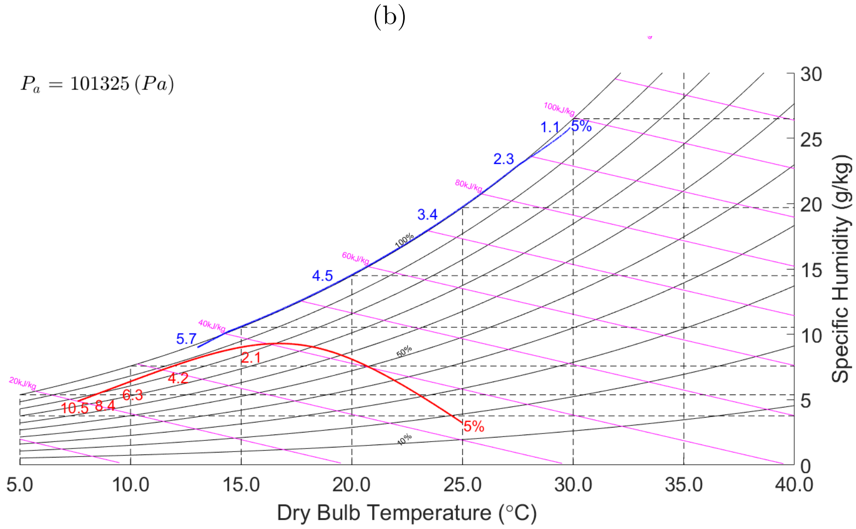

(c)

Figure 3.3: [Color] Non-dimensional plume temperature (panel a) and relative humidity (panel b) as functions of height. Solid curves show the results of a single cooling tower cell, with blue for the inner plume and red for the outer plume. Labels of 5%, 50% and 95% denote the dry air mixing fraction (DAMF).

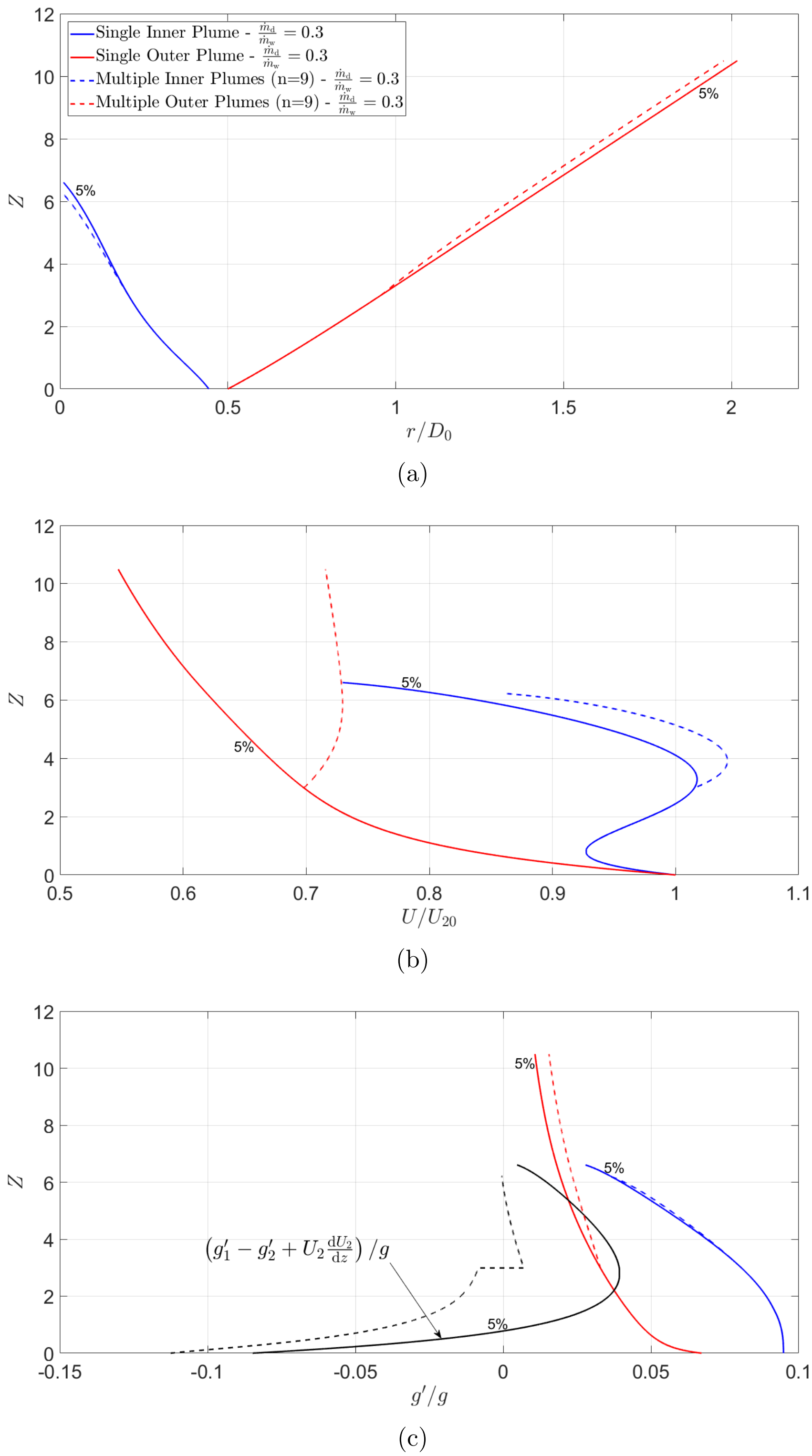

Figure 3.4: [Color] As in figure 3.2 but with $\frac{\dot{m}_{\rm d}}{\dot{m}_{\rm w}} = 0.3$ and 5% DAMF.

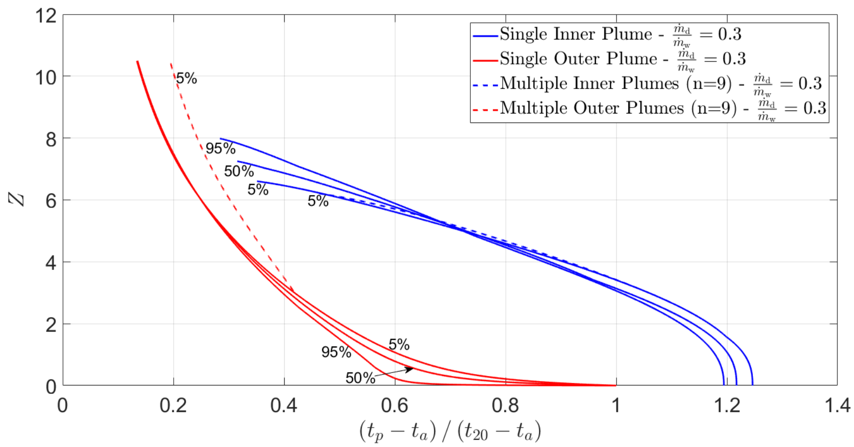

(a)

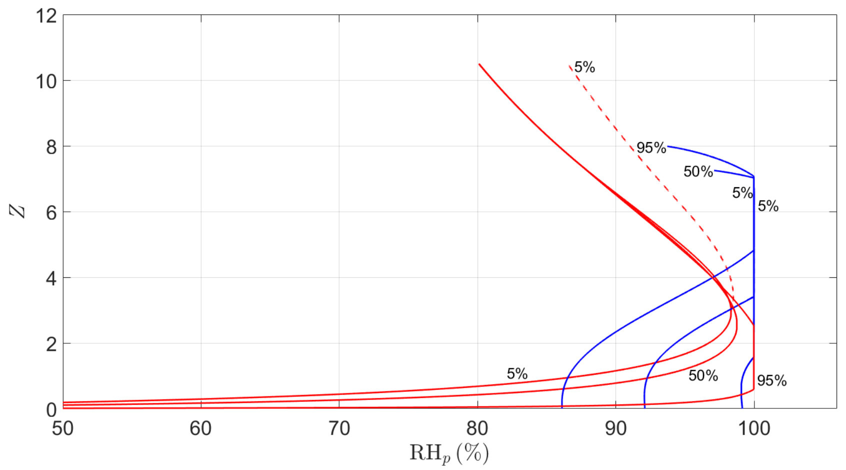

(b)

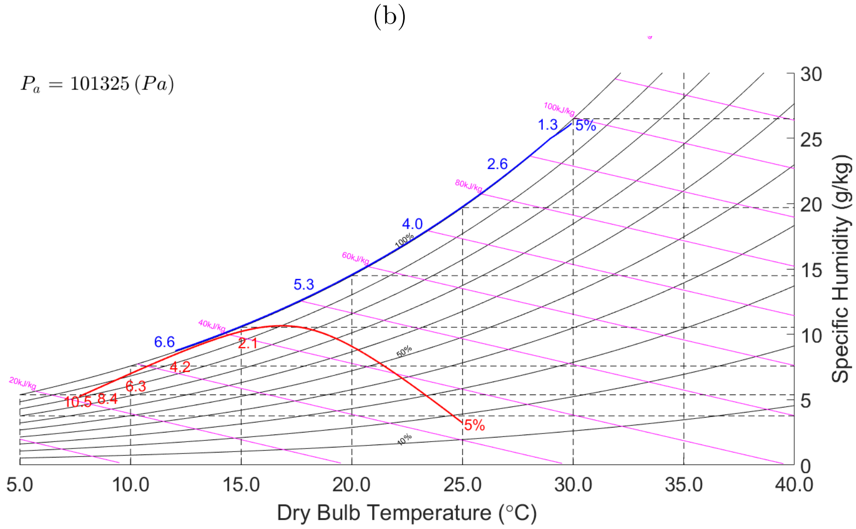

(c)

Figure 3.5: [Color] As in figure 3.3 but with $\frac{\dot{m}_\mathrm{d}}{\dot{m}_\mathrm{w}} = 0.3$.

distinguishable. Figure 3.5 b illustrates that, with 95% DAMF, the outer plume begins to condense at an elevation of $Z = 0.59$, which is less than what is observed in figure 2.3 where condensation is delayed till $Z = 1.21$. However, with 5% or 50% DAMF, there is no condensation in the outer plume throughout the dilution process because the outer plume is relatively thick and the moisture is concentrated in the inner (visible) plume. Besides, visible inner plumes with 5% and 50% DAMF start at $Z = 1.58$ and $Z = 3.42$ respectively, which are both larger than the threshold elevation from figure 2.3.

4 How much mixing should occur in the plenum of a crossflow cooling tower?

4.1 Hybrid cooling tower calculations – the effectiveness-NTU method

Similar to uniform plumes, the behavior of coaxial plumes depends on conditions measured at the source. In assessing the parametric regimes where a coaxial plume may prove advantageous, it is necessary to first understand how the source conditions are influenced by environmental and operating conditions. In this spirit, reference is made to the Examples 8.1.3 and 9.4.1 of Kröger (2004), which respectively consider the wet and dry sections of a PPWD crossflow cooling tower. Using the input parameters summarized in table 4.1, we adapt Kröger's effectiveness-NTU solution methodology along the lines presented in Appendix B. In so doing, we introduce the dry cooling energy fraction or DCEF as the ratio of the dry to wet section range temperatures. Symbolically, DCEF $= (T_{D1} - T_{D2})/(T_{W1} - T_{W2})$ where the temperatures are defined in figure 2.1. As indicated in table 4.1, and consistent with Kröger (2004), we assume DCEF $= 20\%$. Accordingly, our effectiveness-NTU calculations yield output as summarized in table 4.2 from which the coaxial plume equations of section 3 may be integrated forward in Z.

Table 4.1: Input parameters for a hybrid cooling tower calculation.

Variable name and symbol	**Value (unit)**
Ambient pressure at the top of the cooling tower, P_a	101325 (Pa)
Range temperature in the wet section, R_W	10 (°C)
Dry cooling energy fraction (DCEF)	20 (%)
Ambient dry-bulb temperature, t_a	5 (°C)
Ambient relative humidity, RH_a	60 (%)
Water mass flow rate, L	1000 (kg/s)
Liquid-to-air ratio in the wet section, $\frac{L}{G_W}$	1.0
Fill height, H	11 (m)
Fill depth (air travel distance), ATD	4.57 (m)

Table 4.2: Output parameters for a hybrid cooling tower calculation.

Variable name and symbol	**Value (unit)**
Approach temperature in the wet section, A_W	14.2 (°C)
Approach temperature in the dry section, A_D	20.7 (°C)
Wet cooling temperature, t_w	19.0 (°C)
Dry cooling temperature, t_d	18.8 (°C)
Liquid-to-air ratio in the dry section, $\frac{L}{G_D}$	1.66

4.2 Visible plume resistance and recirculation

The "two-thirds law" of Briggs (1969) implies that buoyant inner plumes having large rise velocities are less likely to be deflected by the wind and are therefore less likely to lead to ground level fog and/or a recirculation of moist air through the dry or wet sections of the cooling tower. Efforts have been made to determine empirically the resistance of a (uniform) plume to deflection by the wind – see e.g. figure 9.4.1 of Kröger (2004). Here we follow an alternative approach based on the analytical solutions developed in section 3. First, and whether we wish to consider the inner plume, the outer plume or both, it is necessary to combine the vertical velocity, U, and relative humidity, RH, into a single (non-dimensional) parameter. For this purpose, we define the ratio $\mathcal{R} = \mathcal{R}(Z) = \frac{U/U_{20}}{\mathrm{RH}}$ as the height-dependent *resistance factor*. The name stems from the fact that, as $\mathcal{R}$ increases, the local resistance of the (coaxial) plume to both fog formation and recirculation also increases. Of course, $\mathcal{R}$ does not, in and of itself, indicate when a visible plume will occur. In the event of fog formation, the air is supersaturated with water vapor and for this particular case an equivalent relative humidity must be defined as $\mathrm{RH} = \frac{q_{sp}+\sigma}{q_{sp}}$ (Monjoie and Libert, 1994).

The above ideas are illustrated with reference to the curves of figure 4.1, which derive from the input parameters of table 4.1. The plume velocity and relative humidity are shown in figure 4.1 a. Note that in contrast to figures 3.3 b and 3.5 b, the inner plume relative humidity is here nearly constant with height. Obviously the combination of high vertical velocity and low relative humidity is desired in terms of avoiding condensation and recirculation. Figure 4.1 a confirms that, as expected, the inner (outer) plume becomes less (more) susceptible to fog formation as the DAMF increases. On the other hand, the non-monotone character of the blue and red curves shown in figure 4.1 a make it somewhat difficult to make more precise statements. As a result, we instead draw attention to figure 4.1 b, which shows the vertical variation of $\mathcal{R}$ for the inner and outer plumes for a range of different DAMF. Figure 4.1 b reveals that for the outer plume, $\mathcal{R}$ drops sharply for $0 \leq Z \leq 2$, which is mainly due to the rapid increase in the relative humidity. Thereafter, the rate of change of the resistance factor is more moderate. A similar profile is observed in the inner plume in that $\mathcal{R}$ falls rapidly for $Z < 1$ as a result of the loss of momentum of the inner plume close to the source (c.f. figures 3.2 b and 3.4 b). For $Z \geq 1$, the resistance factor decreases less rapidly. Here, changes of vertical velocity are accompanied by positive or negative changes of relative humidity (c.f. figure 3.3).

Although figures 4.1 a and 4.1 b present a quantitative characterization of the visible plume resistance, the relative dimensions of the inner and outer plumes are not taken into consideration. Such geometric details are important because the continuously expanding outer plume is supposed to make a greater contribution to $\mathcal{R}$ than the decaying inner plume. Taking this consideration into account, we define the plume-average resistance factor as

$$\bar{\mathcal{R}} = \frac{1}{Z_{c,\,5\%}} \int_0^{Z_{c,\,5\%}} \left[\frac{Q_1}{Q_1+Q_2} \frac{U_1/U_{20}}{\mathrm{RH}_1} + \frac{Q_2}{Q_1+Q_2} \frac{U_2/U_{20}}{\mathrm{RH}_2} \right] \mathrm{d}Z \,, \tag{4.1}$$

where $Z_{c,\,5\%}$ is a characteristic reference height and RH_1 and RH_2 are the relative humidities of the inner and outer plumes, respectively. Where necessary, we may also compute average resistance factors for the inner and outer plumes separately. The corresponding equations read

$$\bar{\mathcal{R}}_1 = \frac{1}{Z_{c,\,5\%}} \int_0^{Z_{c,\,5\%}} \frac{U_1/U_{20}}{\mathrm{RH}_1} \mathrm{d}Z \,, \tag{4.2}$$

$$\bar{\mathcal{R}}_2 = \frac{1}{Z_{c,\,5\%}} \int_0^{Z_{c,\,5\%}} \frac{U_2/U_{20}}{\mathrm{RH}_2} \mathrm{d}Z \,, \tag{4.3}$$

Figure 4.1 c illustrates the variation of $\bar{\mathcal{R}}$, $\bar{\mathcal{R}}_1$ and $\bar{\mathcal{R}}_2$ with the DAMF for both single and multiple cell cooling towers. The increase (decrease) of the inner (outer) plume resistance with increasing

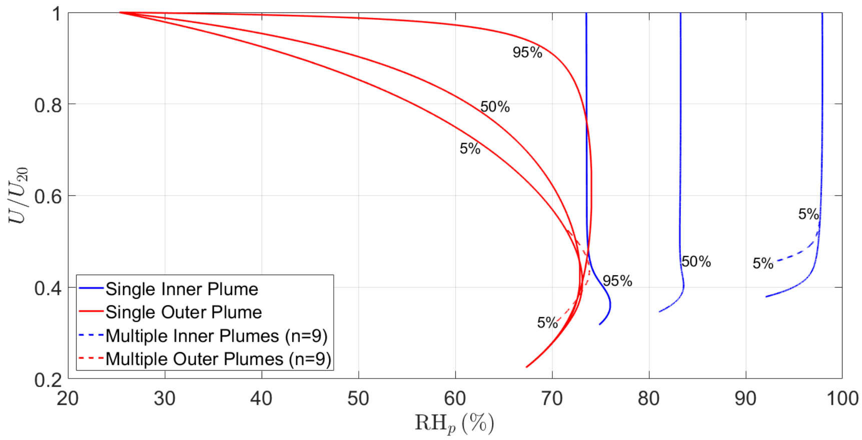

(a)

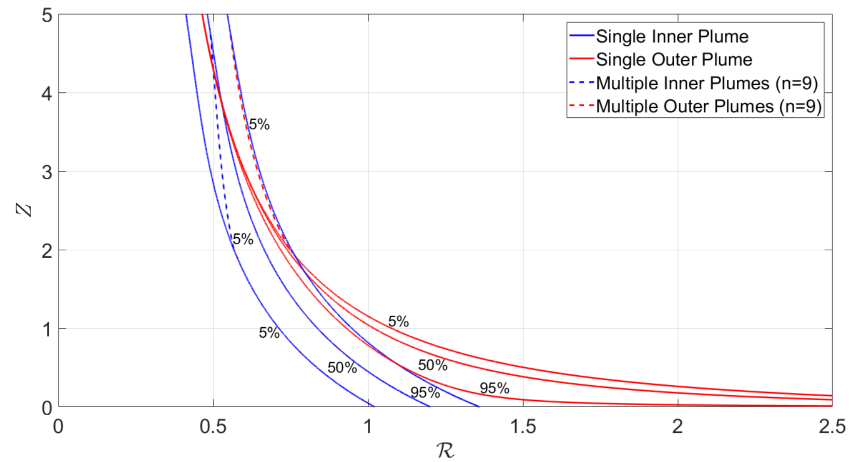

(b)

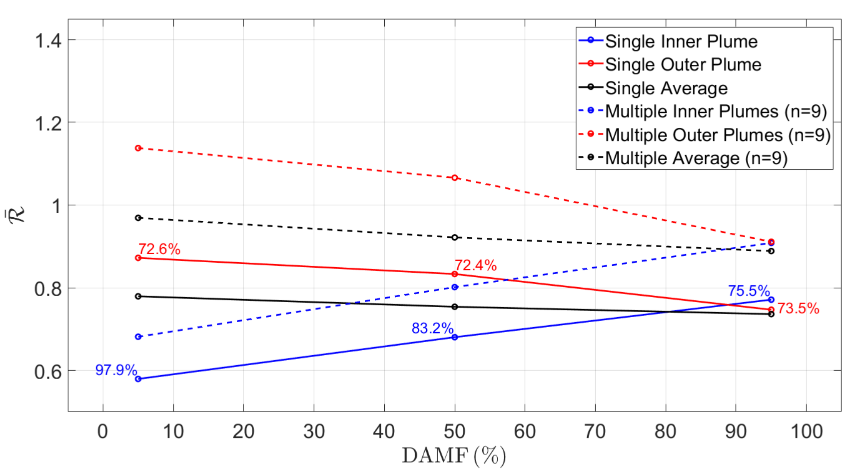

(c)

Figure 4.1: [Color] (a) plume velocity vs. relative humidity. (b) resistance factor vs. height. (c) resistance factor, averaged over height, vs. DAMF. For the single cell case, 5%, 50% and 95% DAMFs are presented, while for multiple cells only 5% DAMF is shown in panels (a) and (b). In panel (c), the maximum relative humidities are specified for select DAMF.

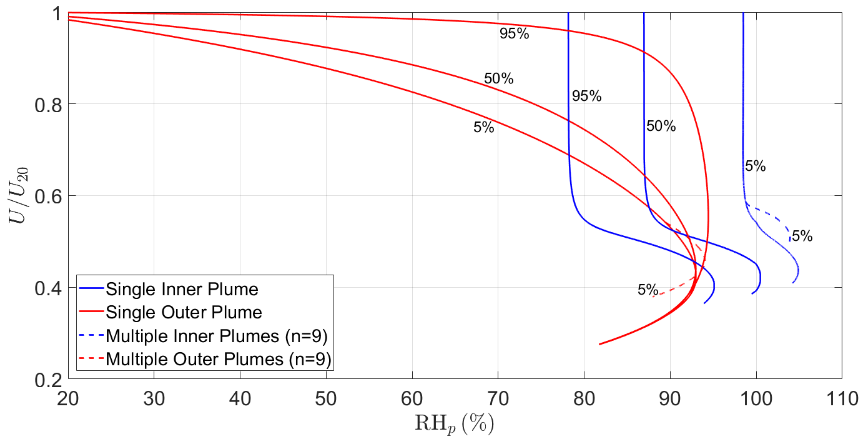

(a)

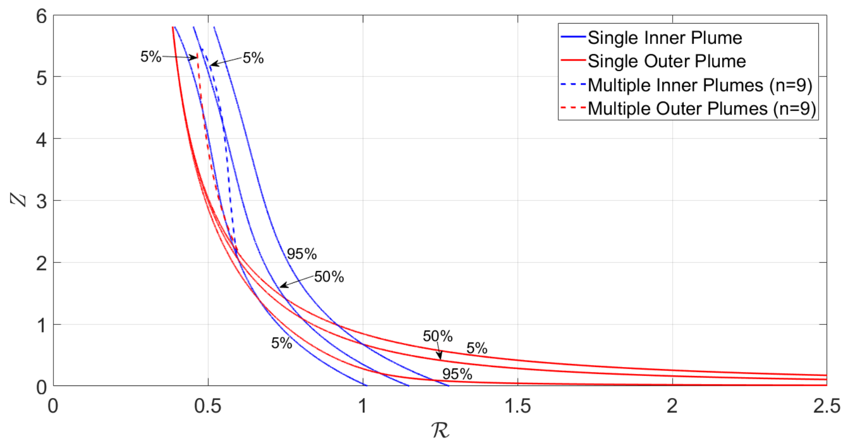

(b)

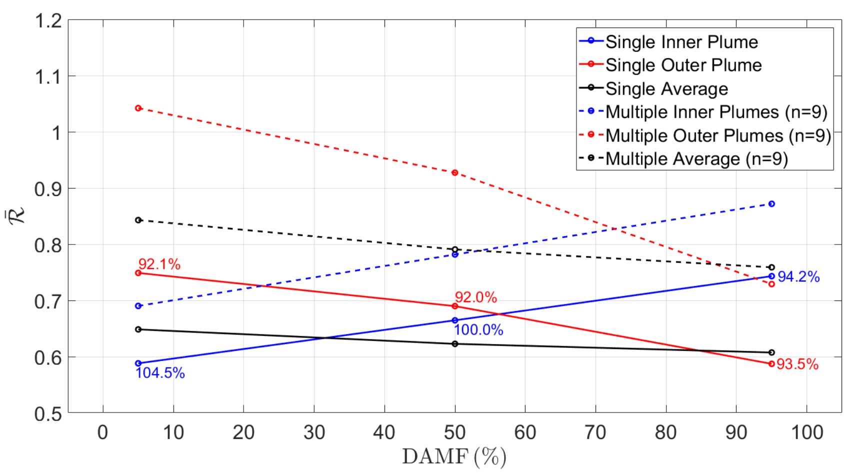

(c)

Figure 4.2: [Color] As with figure 4.1 but with ambient temperature $t_a = -10\,^{\circ}\mathrm{C}$, and other input parameters remain the same in table 4.1.

DAMF has been justified in figure 4.1 a. More importantly, and less intuitively, the black curves of figure 4.1 c indicate that $\bar{\mathcal{R}}$ decreases with the DAMF. This observation is significant because it suggests that, for the plume as a whole, there is a moderate but not inconsequential advantage to limiting the degree of mixing of the wet and dry air streams in the plenum chamber. Of course, this strategy should not be applied absolutely: in the limit of no mixing, the inner plume would be saturated and condensation would occur immediately upon discharge to the atmosphere. As a consequence, it is important when interpreting curves such as those presented in figure 4.1 c to separately evaluate the relative humidities of the inner (and outer) plumes. Such data are presented in blue (and red) text in figure 4.1 c. From the information so provided, we confirm that a maximum (inner plume) relative humidity of 97.9% is realized when, as expected, the DAMF is a minimum. Note finally that figure 4.1 c indicates that merged plumes exhibit larger resistance factors than do individual (axisymmetric) plumes. Insofar as visible plume abatement is concerned, a single plume corresponds to a worse case scenario.

Whereas figure 4.1 is limited to an invisible plume, figure 4.2 extends the previous analysis to the case of a visible plume consisting of supersaturated air. Note that the results of figure 4.2 are obtained by decreasing the ambient temperature t_a in table 4.1 from 5 °C to −10 °C. The relatively low dry-bulb temperature tends to increase the dry cooling efficiency, which results in a low dry air mass flow rate in the dry section, G_D. Correspondingly the inner plume may become saturated, or supersaturated, which is clearly evident in figure 4.2 a. Despite the presence of fog, figures 4.2 b and 4.2 c show qualitatively similar trends to figures 4.1 b and 4.1 c, respectively. In particular, the black curves of figure 4.2 c still show a decreasing trend of $\bar{\mathcal{R}}$ vs. the DAMF. Notwithstanding this observation, it may in this case be disadvantageous to limit the mixing of the wet and dry air streams owing to the large inner plume relative humidities that result. Formalizing this last statement, we propose that the following two criteria must be satisfied in order for a coaxial plume structure to be considered advantageous from the point of view of avoiding fog formation and recirculation:

(i) The relative humidity of the outer plume should not exceed 95% for intermediate DAMF, say 50% DAMF. For the inner plume, it may be tolerable to set a less stringent requirement (e.g. $\mathrm{RH}_1 < 100\%$ for 50% DAMF) owing to the smaller dimension of the inner compared to the outer plume. (Note that the specific numbers used above i.e. 50% DAMF, 100% and 95% RH may be adjusted according to site-specific constraints and the severity of local regulations.)

(ii) $\bar{\mathcal{R}}$ should be a monotone decreasing function of the DAMF (as it is in figures 4.1 c and 4.2 c).

The two design criteria summarized at the end of section 4.2 form the basis for figure 4.3, which shows a regime diagram in the (t_a, RH_a) parameter space. Figure 4.3 can be used to determine where a coaxial plume is or is not advantageous; it suggests that for low ambient temperatures and/or high relative humidities, a relatively high DCEF is required to achieve visible plume abatement.

5 Conclusion and future work

Based on the coaxial jet model of Morton (1962) and the turbulent fountain theory proposed by McDougall (1981) and Bloomfield and Kerr (2000), an analytical model describing coaxial plumes is herein developed. This model assumes "top-hat" profiles for the plume velocity, temperature and humidity. Morton's entrainment assumption is used in which the entrainment into the inner plume scales with the velocity difference between the inner and outer plumes.

Our study is motivated by the possible advantage of using coaxial plumes in the context of visible plume abatement from cooling towers, a topic previously investigated by Houx et al (1978), Lindahl and Jameson (1993), Hensley (2009) and Koo (2016a, 2016b). Central to our investigation

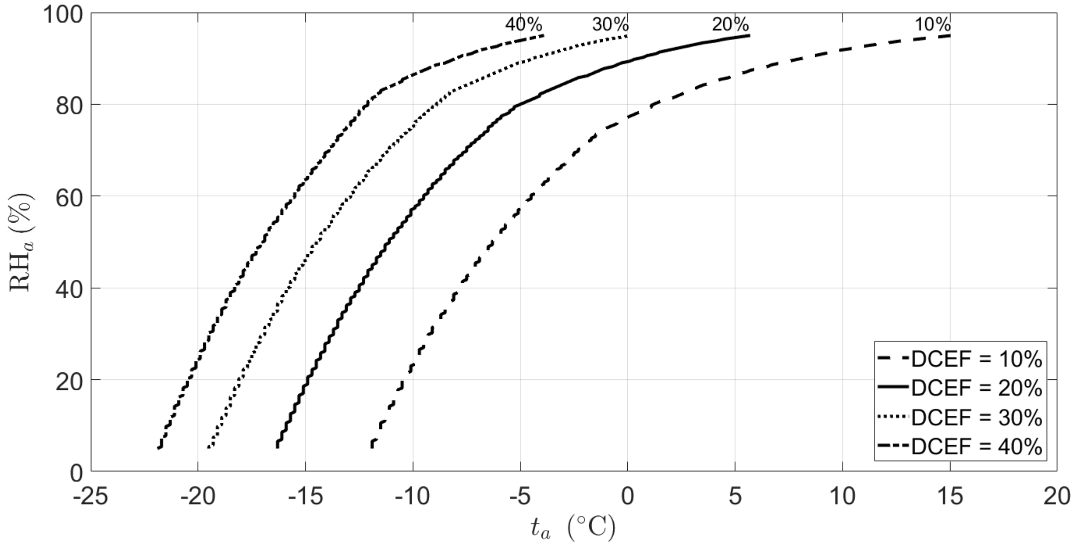

Figure 4.3: Regime diagram indicating the combinations of ambient temperature and relative humidity for which a coaxial plume structure is (to the right of the curves) and is not (to the left of the curves) advantageous. Only single cell results are presented; results for multiple cells are qualitatively similar.

is the notion of partial mixing in the plenum chamber between the wet and dry air streams – see figure 2.5. Our results of section 4.2 are based on the effectiveness-NTU calculations summarized in Appendix B and make reference to a resistance factor $\mathcal{R} = \frac{U/U_{20}}{\mathrm{RH}}$, which characterizes the decreased likelihood of fog formation and/or recirculation. Based on this resistance factor, two criteria are proposed to determine whether a coaxial plume is indeed advantageous as compared to its uniform counterpart. To wit, (i) with 50% DAMF, the respective maximum relative humidities in the inner and outer plume should not exceed 100% and 95%, and, (ii) the resistance factor, averaged over height, should be a monotone decreasing function of the DAMF. On the basis of the aforementioned analyses and criteria, regime diagrams such as figure 4.3 can be drawn in a straightforward fashion. For fixed ambient conditions, such regime diagrams specify whether or not a coaxial plume is likely to be advantageous.

This study opens the door for numerous adaptations and future endeavors. Most immediately, the effectiveness-NTU method summarized in Appendix B is predicated on a number of simplifying assumptions e.g. the humid air exiting the wet section is just saturated i.e. RH = 100%. Relaxing these assumptions could provide a more detailed description of the interior dynamics and, by extension, the plume source conditions and their relationship to key environmental and operational variables. Moreover, laboratory experiments e.g. using a water channel ought to be performed so that the most appropriate values for the entrainment coefficients for α, β and γ may be determined. Indeed, table 3.1 confirms that model output may be sensitive to the value of these entrainment coefficients (β most especially) and so careful estimation of the values seems to us important. Finally, all of the above analysis assumes a still (and, for that matter, uniform-density) ambient. Whereas incorporating the effect of wind is nontrivial from an analytical point of view, good progress might again be possible using laboratory experiment. Of particular interest would be to estimate the threshold wind speed for which the coaxial structure becomes very heavily distorted so that the inner plume is directly exposed to ambient fluid. It is also worthwhile mentioning the differences between the current coaxial plume structure vs. a forced i.e. relatively high velocity (dry) air curtain, the latter of which can lift the wet plume to some nontrivial extent (Veldhuizen and Ledbetter, 1971). Whether, from the point of view of fluid mechanics, economics, etc., one approach is generally favorable to the other remains to be investigated carefully.

6 Acknowledgments

Financial support for the current project was generously provided by Natural Sciences and Engineering Research of Canada (NSERC), International Cooling Tower Inc. and China Scholarship Council (CSC). We sincerely thank our colleagues from International Cooling Tower Inc. for many helpful insights and fruitful discussions.

References

ASHRAE (2013) Fundamentals, si ed. American Society of Heating, Refrigerating and Air Conditioning Engineers: Atlanta, GA, USA

Bloomfield LJ, Kerr RC (2000) A theoretical model of a turbulent fountain. Journal of Fluid Mechanics 424:197–216

Briggs GA (1969) Plume rise usaec critical review series tid-25075. National Technical Information Service, Springfield, Virginia 22161

Briggs GA (1975) Plume rise from multiple sources. Tech. rep., National Oceanic and Atmospheric Administration, Oak Ridge, Tenn.(USA). Atmospheric Turbulence and Diffusion Lab.

Carhart R, Policastro A (1991) A second-generation model for cooling tower plume rise and dispersioni. single sources. Atmospheric Environment Part A General Topics 25(8):1559–1576

Csanady G (1971) Bent-over vapor plumes. Journal of Applied Meteorology 10(1):36–42

Curry JA, Webster PJ (1998) Thermodynamics of atmospheres and oceans, vol 65. Academic Press

Davidson G (1986) Gaussian versus top-hat profile assumptions in integral plume models. Atmospheric Environment (1967) 20(3):471–478

Emanuel KA (1994) Atmospheric convection. Oxford University Press on Demand

Hanna SR (1972) Rise and condensation of large cooling tower plumes. Journal of applied meteorology 11(5):793–799

Hensley J (2009) Cooling tower fundamentals, spx cooling technologies, inc. Overland Park, Kansas USA,

Houx JR, Landon RD, Lindahl Jr PA (1978) Bottom vented wet-dry water cooling tower. US Patent 4,076,771

Hubbard BJ, Mockry EF, Kinney Jr O (2003) Air-to-air atmospheric exchanger for condensing cooling tower effluent. US Patent 6,663,694

Jaber H, Webb R (1989) Design of cooling towers by the effectiveness-ntu method. ASME J Heat Transfer 111(4):837–843

Janicke U, Janicke L (2001) A three-dimensional plume rise model for dry and wet plumes. Atmospheric Environment 35(5):877–890

Kloppers JC, Kröger DG (2005) The lewis factor and its influence on the performance prediction of wet-cooling towers. International Journal of Thermal Sciences 44(9):879–884

Koo JB (2016a) Plume abatement cooling tower. KR Patent 20160007843

Koo JB (2016b) Plume abatement cooling tower. KR Patent 20160109975

Kröger DG (2004) Air-cooled heat exchangers and cooling towers. PennWell Books

Lindahl P, Jameson RW (1993) Plume abatement and water conservation with the wet/dry cooling tower. Tech. rep., Electric Power Research Inst., Palo Alto, CA (United States); Yankee Scientific, Inc., Medfield, MA (United States)

List E (1982) Turbulent jets and plumes. Annual review of fluid mechanics 14(1):189–212

McDougall TJ (1981) Negatively buoyant vertical jets. Tellus 33(3):313–320

Monjoie M, Libert JP (1994) Testing procedures for wet/dry plume abatement cooling towers. CTI JOURNAL 15:56–56

Monteiro E, Torlaschi E (2007) On the dynamic interpretation of the virtual temperature. Journal of the atmospheric sciences 72(9)

Morton B (1957) Buoyant plumes in a moist atmosphere. Journal of Fluid Mechanics 2(02):127–144

Morton B (1962) Coaxial turbulent jets. International Journal of Heat and Mass Transfer 5(10):955–965

Morton B, Taylor G, Turner J (1956) Turbulent gravitational convection from maintained and instantaneous sources. In: Proceedings of the Royal Society of London A: Mathematical, Physical and Engineering Sciences, The Royal Society, vol 234, pp 1–23

Streng A (1998) Combined wet/dry cooling towers of cell-type construction. Journal of energy engineering 124(3):104–121

Takata K, Michioka T, Kurose R (2016) Prediction of a visible plume from a dry and wet combined cooling tower and its mechanism of abatement. Atmosphere 7(4):59

Veldhuizen H, Ledbetter J (1971) Cooling tower fog: control and abatement. Journal of the Air Pollution Control Association 21(1):21–24

Weil JC (1974) The rise of moist, buoyant plumes. Journal of Applied Meteorology 13(4):435–443

Wigley T (1975) A numerical analysis of the effect of condensation on plume rise. Journal of Applied Meteorology 14(6):1105–1109

Wigley T, Slawson P (1971) On the condensation of buoyant, moist, bent-over plumes. Journal of Applied Meteorology 10(2):253–259

Wigley T, Slawson P (1972) A comparison of wet and dry bent-over plumes. Journal of Applied Meteorology 11(2):335–340

Wu FH, Koh RC (1978) Mathematical model for multiple cooling tower plumes, vol 1. Environmental Protection Agency, Office of Research and Development, Environmental Research Laboratory

A Plume merger

A.1 Uniform plumes

The (vertically ascending) plumes discharged from cooling tower cells are assumed to be axisymmetric. When, as is typical, there are multiple cooling tower cells, adjacent axisymmetric plumes merge relatively quickly, where the precise vertical distance obviously depends on the cell spacing. As shown in figure A.1, the cross-sectional area of the resulting merged plume tends to be elliptical. Here, we adopt the merging criteria used by Wu and Koh (1978). Accordingly, plume merger is assumed to initiate once the area of the central rectangle from figure A.1 equals the areas of the two half round circles indicated by the dashed lines.

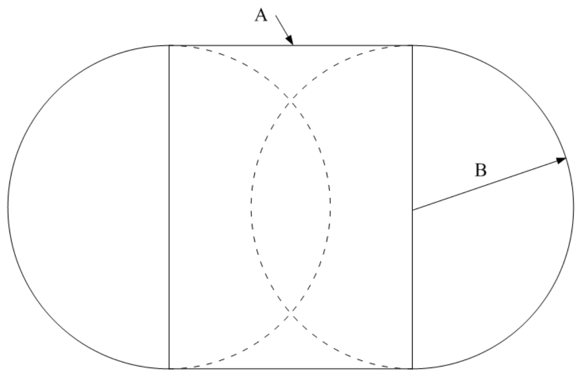

Figure A.1: A cross-sectional view of the merged plume shape. The dashed circles represent the individual plumes at the moment that the merging criterion is satisfied and the solid curve shows the geometry of the merged plume.

Up to the point of merger, the equations for individual round plumes are applied to calculate relevant properties such as the plume temperature, moisture, vertical velocity and width. Once merging occurs we then determine the new centroid and shape of the merged plume, the latter being necessary to estimate the perimeter, S, and the rate of ambient entrainment – see (2.5). Moreover, the fluxes of the merged plumes are summed in order to respect e.g. conservation of mass.

The merged plume is characterized by the width, A, of the central rectangle and the radii, B, of the half circles – see figure A.1. Whereas the radii of the the half circles are the same as the radii of the individual plumes, A can calculated based on geometric considerations, i.e.

$$A = \frac{\pi B}{2}\,, \tag{A.1}$$

Once the shape of the merged plume is determined, solutions for the line and half-round plumes are integrated forward by one spatial step. Because of the different entrainment rates for the line and half-round plumes, the new radii, b, of the half round plumes and the width, a, of the central line plume may be inconsistent in that a non-smooth shape is predicted for the plume cross-section (see the dashed line of figure A.2). In order to correct this model deficiency, the following equations are proposed:

$$\pi b^2 U_r + 2baU_l = \left(\pi B^2 + 2AB\right) U\,, \tag{A.2}$$

$$a + 2b = A + 2B\,, \tag{A.3}$$

where U_r, U_l, and U are, respectively, the plume velocities corresponding to the half-round plumes with radii b, the line plume with width a, and the modified merged plume shape defined by B and A. Equation (A.2) describes a redistribution of the volume flux from the calculated merged plume to the modified merged plume indicated by the solid line in figure A.2. Conversely, (A.3) ensures the same plume width between the calculated and modified plumes.

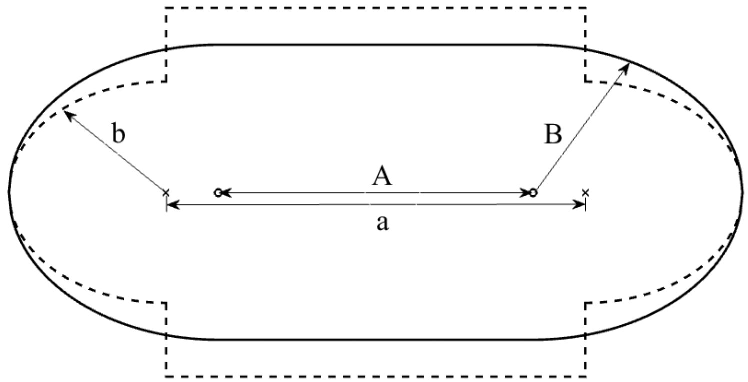

Figure A.2: A cross-sectional view of the modified shape of the merged plume.

A.2 Coaxial Plumes

Plume merger involving coaxial plumes is more complicated than in section A.1; nonetheless, similar principles can be applied. Upon merger, and as illustrated schematically in figure A.3, the outer plumes coalesce with each other to become a single plume characterized by a slot plume in the center and two half round plumes at the two ends. The inner plumes (if they still exist) remain discrete because the radii of inner plumes shrink with elevation. For computational tractability, we manually shift the two terminal inner plumes inwards so as to avoid an uneven division between the central slot plume and two half round plumes. This assumption seems to be justified based on expectations of flows characterized by entrainment. Moreover, it applies only to the two end member inner plumes; no such translation is required for those inner plumes (seven in the case of figure 2.5) that are not adjacent to an end of the line plume.

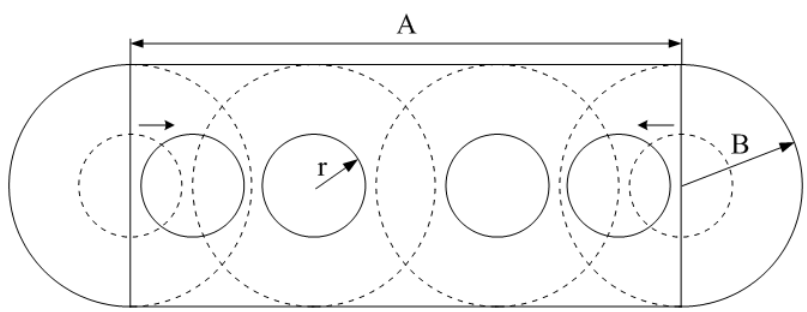

Figure A.3: A cross-sectional view of four coaxial plumes upon merging. The solid curves or circles represent the merged coaxial structure.

B Hybrid wet/dry cooling tower calculation

This section gives a description of the effectiveness-NTU method for crossflow dry and wet sections, and illustrates how the hybrid cooling tower calculation is implemented.

B.1 Effectiveness-NTU method for a crossflow dry section

The geometric parameters in the dry section are drawn from Example 9.4.1 in Kröger (2004). The heat capacity rates are defined as

$$[C_{min}, C_{max}] = \begin{cases} [L\,C_{pw}, G_W\,C_{pa}] & \text{if } L\,C_{pw} < G_W\,C_{pa} \\ [G_W\,C_{pa}, L\,C_{pw}] & \text{otherwise} \end{cases}$$

and the heat capacity ratio is $C_R = C_{min}/C_{max}$. The maximum heat transfer rate is

$$Q_{max} = C_{min}\left(T_{D1} - t_a\right) . \tag{B.1}$$

Given the range temperature in the dry section, R_D, the effectiveness in demand, ϵ_d, is given by

$$\epsilon_d = L\,C_{pw}\,R_D/Q_{max} , \tag{B.2}$$

Meanwhile, the number of transfer units per pass is

$$\mathrm{NTU}_p = \frac{U_i\,A_i}{C_{min}\,n_p} , \tag{B.3}$$

where n_p is the number of water passes, U_i is the overall heat transfer coefficient based on the total inside area, A_i, of the tubes. Note that U_i and A_i are calculated primarily based on the dry section geometrical parameters. If, as recommended by Jaber and Webb (1989), we assume that both streams i.e. air and water flows are unmixed[4], the effectiveness per pass is

$$\epsilon_p = 1 - \exp\left[\mathrm{NTU}_p^{0.22}\left(\exp\left(-C_R\,\mathrm{NTU}_p^{0.78}\right) - 1\right)/C_R\right] . \tag{B.4}$$

From ϵ_p, it is straightforward to compute the total effectiveness in supply from

$$\epsilon_s = \left[\left(\frac{1-\epsilon_p\,C_R}{1-\epsilon_p}\right)^{n_p} - 1\right] \Big/ \left[\left(\frac{1-\epsilon_p\,C}{1-\epsilon_p}\right)^{n_p} - C_R\right] . \tag{B.5}$$

The operating point is determined by equating ϵ_s and ϵ_d using the iteration process outlined in figure B.1.

B.2 Effectiveness-NTU method for a crossflow wet section

The detailed derivation of effectiveness-NTU theory for the wet section is outlined in Chapter 4 of Kröger (2004), where canonical fill characteristics are drawn from Kröger's Example 8.1.3. The enthalpy-temperature gradient is approximated as

$$\frac{\mathrm{d}i_{sw}}{\mathrm{d}T_W} = \frac{i_{sw,1} - i_{sw,2}}{T_{W1} - T_{W2}} , \tag{B.6}$$

where $i_{sw,1}$ and $i_{sw,2}$ are the respective saturated air enthalpies at water temperatures T_{W1} and T_{W2}. Consistent with the dry heat exchanger design process, the heat capacity rates are defined as

$$[C_{min}, C_{max}] = \begin{cases} [L\,C_{pw}/\left(\mathrm{d}i_{sw}/\mathrm{d}T_W\right), G_W] & \text{if } L\,C_{pw}/\left(\mathrm{d}i_{sw}/\mathrm{d}T_W\right) < G_W \\ [G_W, L\,C_{pw}/\left(\mathrm{d}i_{sw}/\mathrm{d}T_W\right)] & \text{otherwise} \end{cases}$$

and the evaporative capacity rate ratio is given as $C_R = C_{min}/C_{max}$. The maximum enthalpy transfer is

$$Q_{max} = C_{min}\left(i_{sw,1} - \lambda - i_a\right) , \tag{B.7}$$

[4] As stated in Kröger (2004), unmixed flow indicates that the temperature variations within the fluid in at least one direction normal to the flow can exist but no flux of heat occurs.

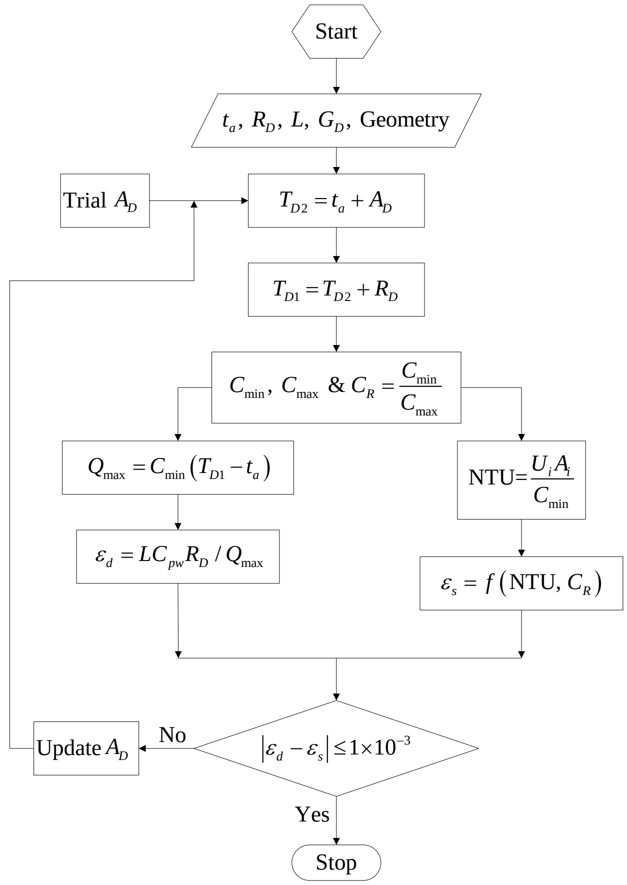

Figure B.1: The dry section calculation diagram.

where the correction factor λ is defined as $\lambda = \left(i_{sw,1} + i_{sw,2} - 2\, i_{sw,m}\right)/4$, and $i_{sw,m}$ is the saturated air enthalpy at the mean water temperature $\left(T_{W1} + T_{W2}\right)/2$. Given the range temperature in the wet section, R_W, the effectiveness in demand, ϵ_d, is expressed as

$$\epsilon_d = L\, C_{pw}\, R_W / Q_{max}\,, \tag{B.8}$$

Meanwhile, the fill transfer coefficient per meter of fill height (H) is given as

$$\frac{h_d\, a_{fi}}{L'} = C \left(\frac{L'}{G'_W}\right)^{-n}, \tag{B.9}$$

where h_d is the mass transfer coefficient, a_{fi} is the wetted surface area divided by the volume of the fill, $L' = L/A_{fr,h}$ is the mean water mass flow rate through the fill with $A_{fr,h}$ the horizontal frontal area of the fill, $G'_W = G_W/A_{fr,v}$ is the mean air mass flow rate with $A_{fr,v}$ the vertical frontal area of the fill, and C and n are empirical constants here set to 0.268 and 0.56, respectively (Table 4.3.2a of Kröger, 2004). The number of transfer units (NTU) is given as

$$\text{NTU} = \frac{h_d A}{C_{min}}\,, \tag{B.10}$$

where $A = a_{fi}\, V$ is the total wetted surface area in the fill and V is the volume of the fill. By simple rearrangement, (B.10) can be expressed as $\text{NTU} = \frac{h_d\, a_{fi}}{L'}\, \frac{L\, H}{C_{min}}$, thus the fill transfer coefficient can be related to the NTU. The effectiveness-NTU equation for crossflow with both streams unmixed is given as

$$\epsilon_s = 1 - \exp\left[\text{NTU}^{0.22}\left(\exp\left(-C_R\, \text{NTU}^{0.78}\right) - 1\right)/C_R\right]. \tag{B.11}$$

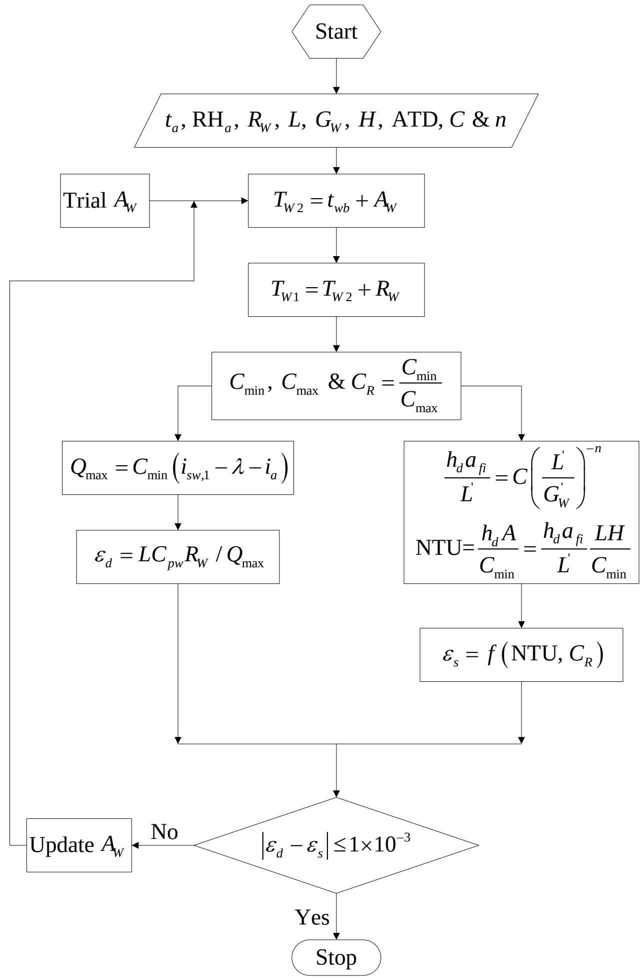

Figure B.2: The wet section calculation diagram.

The determination of the wet section operating point is similar to that of the dry section in that ϵ_s and ϵ_d must be matched. The corresponding calculation flowchart is shown in figure B.2.

B.3 The PPWD crossflow cooling tower calculation

The calculations to be performed for a hybrid PPWD crossflow cooling tower must obviously incorporate those from the previous two subsections. Accordingly, the flowchart of figure B.3 makes reference to both figures B.1 and B.2. Because the water flows in both the dry and wet sections are in series, the restriction, $T_{D2} = T_{W1}$, must be invoked in the PPWD crossflow calculation. Therefore, if the dry air mass flow rate in the wet section, G_W, is fixed, the dry air mass flow rate in the dry section, G_D, is supposed to be solved using the a trial-and-error approach suggested in figure B.3.

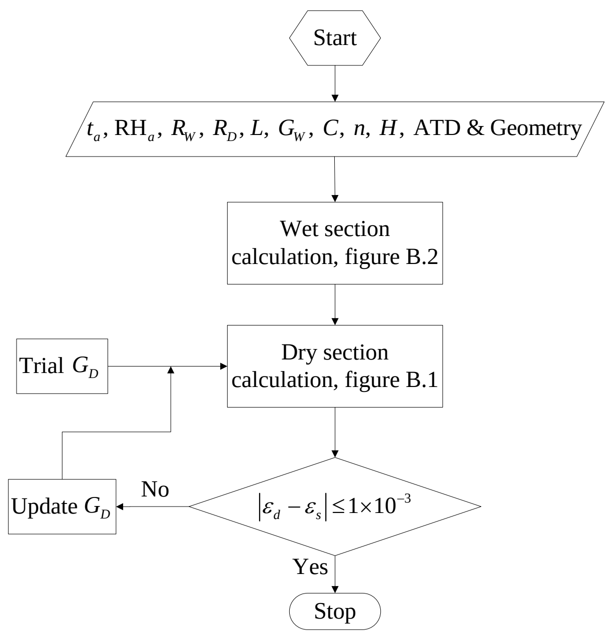

Figure B.3: The PPWD crossflow tower calculation diagram.